

Testing Planck 2020 and DESI data on w CDM Models

Kathleen Sammut^{1,2,*}

¹*Institute of Space Sciences and Astronomy, University of Malta, Msida, Malta*

²*Department of Physics, University of Malta, Msida, Malta*

This work delves into the dynamical dark energy models of the w CDM parameterisation that are defined by their equation of state by comparing different, well-known parameterisation models, in an attempt to lessen the tensions of H_0 and σ_8 by using the latest observational data. This research also tested the newer Planck likelihood and BAO data by comparing them to their predecessors. The data that was used were: the Cosmic Microwave Background (CMB) data of Planck 2018 and Planck 2020 data; Cosmic Chronometers (CC), a sample of Supernovae Type Ia; and Baryonic Acoustic Oscillations (BAO). A Bayesian analysis was performed to produce the results needed for the analysis. From the analyses, the best-fit values of the parameters show that almost all models are in favour of a phantom Universe. This study also showed that the new tested data constrained the models better than the previous ones, while also showing that the observation data supports the Λ CDM model over the dynamical dark energy models.

Keywords: w CDM, DESI, Planck 2020, Hubble Tension, Sigma 8 Tensions

1. INTRODUCTION

During this last decade, the cosmic tension has been continuously debated in modern cosmology as discrepancies between the values of the Hubble parameter, H_0 , [1] and the amplitude of the matter power spectrum, σ_8 , [2] derived either indirectly, through the use of models or directly, through standard candles [3, 4], still persist. This gave rise to the possibility of an alternative model to the standard model. According to observational evidence, the Λ Cold Dark Matter (Λ CDM) [5] cosmology is considered the most well-suited model for explaining the Universe. It presumes that the cosmological constant, Λ , is responsible for driving the accelerated expansion of the Universe. However, despite its success in describing the late accelerating phase, Λ CDM faces several significant challenges. Apart from the tensions with the H_0 [6, 7] and σ_8 , the standard model also has problems regarding the cosmological constant problem, which highlights the discrepancy between the observed small value of the cosmological constant and the large theoretical value predicted by quantum field theory. Furthermore, Λ cosmology fails to address the cosmic coincidence problem, further emphasising the need for alternative explanations or modifications to the model. This further pushes the scientific community to search for an alternative model that might lessen or even remove the problems found in the standard model of cosmology [8].

To explain the phenomenon of H_0 , two main approaches have been proposed: one involves keeping to the theory of general relativity while introducing new components that go beyond the Standard Model of Particle Physics [9, 10]; the other involves constructing modified theories of gravity that contain additional degrees of freedom from which one can derive the Universe's expansion rate. Since the Universe is assumed to be a fluid, both approaches lead to a value of the expansion rate of the Universe that is affected by the evolution of the dark energy equation of state, w . This parameter w , represents the ratio of the dark energy's pressure, p , to its energy density, ρ . The standard model takes the assumption that $w = -1$, meaning that the Universe behaves like a dark energy fluid due to it being negative. The simplest generalisation of the Λ CDM model is to relax the assumption that w is -1 throughout the history of the Universe, known as the w CDM model [11, 12]. The first approach to this is taking w to be a constant, but $w \neq -1$ [13]. However, a better generalisation of the standard model would be one that considers the equation of state to be time-dependent. This can be done by parameterising w in terms of the cosmological redshift with the use of different functional forms. This gives more freedom to reconstruct the expansion history of the Universe with respect to the observational data.

* kathleen.sammut.19@um.edu.mt, ksamm09@um.edu.mt, kathsammut27@gmail.com

In the literature, many different dark energy models can be found that fit the observational data: there are one-parameter models, such as the constant model; two-parameter models, namely, Chevallier-Polarski-Linder parametrization [14, 15], Jassal-Bagla-Padmanabhan parametrisation [16, 17], Logarithmic parametrisation [18], and oscillatory parameterisation models [19, 20]; three-parameter models [21]; and four-parameter parameterizations [12, 21, 22]. w CDM models received significant attention when recent studies suggested that observational data favoured a dynamic dark energy equation of state. As precision measurements keep advancing and observational data becomes more precise, the need to explore different dark energy equation of state models becomes more pressing.

New cosmic microwave background data (CMB) and Baryonic Acoustic Oscillations (BAO) data sets, Planck 2020 and DESI, were released in 2022 and 2024, respectively. Since these two data sets are still considered new, rigorous testing needs to be done on them to make sure that these data sets can be trusted for the testing of models. In this study, the examination of six popular dark energy models that are characterised by their equation of state will be carried out with the help of CMB data of Planck 2018 [2, 23] and Planck 2020 [24], late-time data of CC [25] and SN+SH0ES [26, 27] and BAO [28] data. Beyond deriving cosmological constraints on these proposed parametrisations, the aim is to evaluate whether these models can address the Hubble constant and the sigma tensions. This study will also test the new Planck and DESI data by comparing them to their predecessors.

This paper has been sectioned in the following way. In section 2, the w CDM model will be explained by its background and perturbation equations as well as showcasing the chosen models by their equation of state. In section 3, the chosen observation data that was used in the analysis will be presented. Section 4, displays all the results that were obtained from this study. In section 5, the analysis of the observational constraints on the parameter space of the w CDM models and the comparison of the data set will be carried out. Finally, section 6, closes off with a brief summary of all the results and conclusions that were made through this study.

2. w CDM MODELS

The background and perturbation equations are the integral part of any model. The background equations assume an isotropic and homogeneous Universe. However, at lower scales or high modes, the cosmological principle no longer applies; therefore, the perturbation equations handle the fluctuations that are found in the Universe, such as density and gravitation. Starting from the background equations, the metric is what is known as the Friedmann-Lemaître-Robertson-Walker (FLRW) metric,

$$ds^2 = -dt^2 + a^2(t) \left[\frac{dr^2}{1 - kr^2} + r^2(d\theta^2 + \sin^2 \theta d\phi^2) \right], \quad (1)$$

where $a(t)$ represents the scale factor and t, θ, ϕ are to comoving coordinates in polar form. k can be $-1, 0$ and $+1$ depending on whether an open, flat or closed Universe is considered. In this study, a flat Universe is assumed a priori as it is favoured by observational data. By using the FLRW metric, the Einstein Field equations, and the stress-energy momentum tensor, the first and second Friedmann equations can be derived as,

$$H^2 = \frac{8\pi G}{3} \rho_{tot} \quad (2)$$

where H is the Hubble parameter and is defined as $H = \frac{\dot{a}}{a}$, where the dot represents the derivative with respect to cosmic time t . ρ_{tot} represents the total density of the Universe for all the different types of matter. The second Friedmann equation is derived from the Einstein field equations and the stress-energy tensor and has the form,

$$\frac{\ddot{a}}{a} = \frac{-4\pi G}{3} (\rho_i + 3P_{tot}), \quad (3)$$

where P_{tot} is the total pressure for all different types of matter. Each type of matter is assumed not to mutually interact, then each type of matter is separately conserved. Therefore, each type of matter satisfies

the continuity equation, which is the conservation of energy for an expanding Universe, and is derived from the first law of thermodynamics as,

$$\dot{\rho} + 3H(1 + w_i)\rho_i = 0 , \quad (4)$$

where $w_i \equiv \frac{P_i}{\rho_i}$ is the equation of state parameter and i denotes the type of matter. From the continuity equation, the density of radiation, baryonic matter, cold dark matter, and dark energy can be found. Since radiation has $w_r = \frac{1}{3}$, then $\rho_r \propto \left(\frac{a}{a_0}\right)^{-4}$. In the case of baryonic and cold dark matter, $w_b = 0$ and $w_c = 0$, therefore, $\rho_b \propto \left(\frac{a}{a_0}\right)^{-3} = \rho_c$ [17] where a_0 is the value of the scale factor at current times. Since, dark energy is no longer taken as a constant, like in the standard model, the density of dark energy also needs to be calculated by using the continuity equation [20].

$$\rho_\Lambda = \rho_{\Lambda_0} \left(\frac{a}{a_0}\right)^{-3} \exp\left(-3 \int_{a_0}^a \frac{w_\Lambda(a')}{a'} da'\right) \quad (5)$$

By substituting the densities into the Friedmann equation, we obtain the complete Friedmann equation of w CDM models,

$$H^2 = \frac{8\pi G}{3} \left[\rho_{r_0} a^{-4} + \rho_{b_0} a^{-3} + \rho_{c_0} a^{-3} + \rho_{\Lambda_0} \left(\frac{a}{a_0}\right)^{-3} \exp\left(-3 \int_{a_0}^a \frac{w_\Lambda(a')}{a'} da'\right) \right] , \quad (6)$$

where ρ_{r_0} , ρ_{b_0} , ρ_{c_0} and ρ_{Λ_0} are the present day densities of radiation, baryonic matter, cold dark matter and dark energy, respectively. Moving on to the perturbation equations, even though the w CDM model has the same form of perturbation equations as the standard model [29]. However, the w CDM model still impacts the perturbed space. The perturbed FLRW metric when taking the synchronous gauge is represented as,

$$ds^2 = a^2(\tau)[-d\tau^2 + (\delta_{ij} + h_{ij})dx^i dx^j] , \quad (7)$$

where τ is the conformal time, h_{ij} and δ_{ij} are respectively the perturbed and unperturbed metric [20], which can include scalar, vector, and tensor components. From the perturbed FLRW and the stress-energy momentum tensor, the perturbed continuity equation and the perturbed Euler equation can be derived [30, 31],

$$\delta'_i = -(1 + w_i) \left(\theta_i + \frac{h'_i}{2} \right) - 3\mathcal{H} (c_s^2 - w_i) \delta_i - 9\mathcal{H}^2 \left(\frac{\delta P_i}{\delta \rho_i} - c_{a,i}^2 \right) (1 + w_i) \frac{\theta_i}{k^2} , \quad (8)$$

$$\theta'_i = -\mathcal{H} \left(1 - 3 \frac{\delta P_i}{\delta \rho_i} \right) \theta_i + \frac{\delta P_i}{\delta \rho_i} \frac{1}{1 - w_i} k^2 \delta_i - k^2 \sigma_i . \quad (9)$$

In Eq. 8 and Eq. 9, the prime denotes differentiation with respect to the conformal time $\tau = \int \frac{dt}{a(t)}$. The density perturbation is represented by $\delta_i = \frac{\delta \rho_i}{\rho_i}$, the conformal Hubble parameter is represented as $\mathcal{H} = \frac{a'}{a}$, $h = h_{ij}$ is the trace of the metric perturbations h_{ij} , the divergence of the i th fluid velocity is denoted by $\theta_i \equiv ik^j v_j$, c_s^2 is the sound speed for an imperfect fluid and it is defined as $c_s^2 \equiv \frac{\delta P_i}{\delta \rho_i}$, σ_i is the anisotropic stress of the fluid, which will be neglected in the analysis and $c_{a,i}^2$ is the adiabatic speed of sound [32]. Therefore, $c_{a,i}^2$ can be related to w_i with the equation [33],

$$c_{a,i}^2 = w_i - \frac{w'_i}{3\mathcal{H}(1 + w_i)} . \quad (10)$$

Thus, for any equation of state $w(a)$, the Friedmann equation and the adiabatic speed of sound [34] can be calculated. In this study, four well-known w CDM parameterisations were considered;

- **Parameterisation 1:** The simplest generalisation considered in this study involved assuming that $w(a)$, the dark energy equation of state parameter, is a constant value that is not equal to -1 . This slight deviation from the Λ CDM model introduces a more flexible framework for understanding dark energy. The equation of $w(a)$ that represents this representation is given as:

$$w_{wCDM}(a) = w_{0,wCDM} . \quad (11)$$

This generalisation is often referred to as the constant model and serves as a baseline for comparison with dynamical dark energy equation of state models.

- **Parameterisation 2:** For the exploration of non-linear dynamical dark energy equation of state, a quadratic parameterisation was taken as,

$$w_{JBP}(a) = w_{0,JBP} + w_{a,JBP} a(1-a) . \quad (12)$$

This parameterisation was proposed by Jassal-Bagla-Padmanabhan [16] and is known as the JBP parameterisation. This model incorporates a quadratic term that accounts for more complex dynamical behaviour, potentially offering a better fit to observational data.

- **Parameterisation 3:** A logarithmic model for the dark energy equation of state was proposed by G. Efstathiou [18], describing a different type of evolution for $w(a)$. The equation is expressed as,

$$w_{GE}(a) = w_{0,GE} - w_{a,GE} \ln(a) . \quad (13)$$

This parameterisation was used in this study and will be referred to as the logarithmic model. This logarithmic parameterisation diverges from the polynomial approaches, focusing instead on a logarithmic evolution.

- **Parameterisation 4:** Lastly, an alternative parameterisation is an oscillatory model for the dark energy equation of state. Proposed by Zhang and Ma [19], suggests an oscillatory equation of state and is expressed as,

$$w_{OSCILL}(a) = w_{0,OSCILL} + w_{a,OSCILL} \left[a \sin\left(\frac{1}{a}\right) - \sin(1) \right] . \quad (14)$$

This oscillatory parameterisation explores the possibility of a $w(a)$ that exhibits periodic oscillations over the cosmic time.

In all the above parameterisations, the term $w_{0,i}$ represents the current value of $w(a)$ for the specific model i , while $w_{a,i}$ characterize the evolution of $w(a)$ as a function of the scale factor. These models share the property of having a constant dark energy equation of state at the early Universe, to then transition to more dynamic behaviour as the Universe evolves and moves to late times. This diversity in parameterisations enables a comprehensive analysis of different possible dark energy behaviours.

3. OBSERVATIONAL DATA SAMPLES

In this section, the cosmological data sets that were used in this study will be outlined, describing the statistical methodology employed to constrain the dynamical dark energy models considered in this study.

- **Cosmic Microwave Background (CMB) data from Planck 2020:** The latest Planck CMB data was taken in this study, giving rise to the opportunity for testing the newer dataset. CMB temperature and polarisation anisotropies are taken along with their cross-correlations, including high and low multipoles l . The low- l temperature anisotropies (TT) data were taken from the Lollipop data, using the multipole range of $l < 30$. Since Lollipop only has temperature data, the polarisation data of Planck 2018 [2], for low multipoles, was used for a complete analysis of the data and the chosen models. Hillipop was used for the high multipole range data of $l = 30 - 2500$ [24]. This includes: polarisation anisotropies; temperature anisotropies; and their cross-correlations (TT+ET+EE). The data was accessed via the publicly available Planck likelihood, which marginalises over various nuisance parameters associated with the measurements. For more information, we refer the reader to [24]. Throughout this study, this dataset will be referred to as PR4.
- **Cosmic Microwave Background (CMB) data from Planck 2018:** In addition to the latest CMB measurements in temperature and polarisation from Planck 2020, earlier observations from Planck 2018 were incorporated for a comparison of the analysis. This comparison enables us to assess the differences and impacts arising from the old and new CMB datasets. The complete data on temperature,

polarisation, and cross-correlations of Planck 2018 will be taken for the low and high multipole ranges. Similar to PR4, this CMB data set takes l to be in the range of $2 - 29$ for low- l EE and low- l TT. On the other hand, for high- l TT+TE+EE, Planck 2018 uses the range of $30 \leq l \leq 2508$ for TT and $30 \leq l \leq 1996$ for TE and EE. This dataset will be referred to as PR3 throughout this study.

- **Cosmic Chronometers (CC) data:** The latest Cosmic Chronometers data was used, which consists of 30 data points of H_0 across the range of $0 < z < 2$ [35, 36], utilizing massive, passively evolving galaxies in the Universe, referred to as cosmic chronometers. These measurements are highly precise, obtained through the spectroscopic method, and are independent of any specific model. This data was compiled in [25, 37]. The χ^2 statistic for the cosmic chronometer dataset is expressed as follows:

$$\chi_{CC}^2 = \sum_{i=1}^{30} \frac{(H(z_i) - H_{th}(z_i))^2}{\sigma_i^2}, \quad (15)$$

where each z_i with its corresponding uncertainty σ_8 can be found in Table 4 of [37]. This data will be referred to as the CC data.

- **Supernovae Type Ia from Pantheon+ (SN+) and Supernova H0 for the Equation of State (SH0ES):** Pantheon+ (SN+) [38] is an updated data set of Pantheon (SN). It is a compilation of 1701 light curves of 1550 Type Ia supernovae data points ranging from $0.001 \leq z \leq 2.26$. The updated SN+ data set incorporates improvements in calibration, reduction of systematic errors, and a more comprehensive range of supernovae compared to its predecessor. A prior from the Supernova H0 for the Equation of State (SH0ES) project [27] was considered. This prior obtained a value of 73.04 ± 1.04 $\text{Km s}^{-1}\text{Mpc}^{-1}$ for H_0 , which was calculated using Cepheid variable stars in the host galaxy of 42 Type Ia supernovae. The incorporation of the SH0ES prior to the SN+ data set combines high-redshift supernova data with local measurements, leading to more accurate and reliable measurements of H_0 . The SN+ data with the SH0ES prior has the combined likelihood of,

$$\chi^2 = \Delta D^T (Cov_{stat+sys}^{SN+} + Cov_{stat+sys}^{SH0ES})^{-1} \Delta D, \quad (16)$$

where $Cov_{stat+sys}^{SN+}$ and $Cov_{stat+sys}^{SH0ES}$ are the statistical and systematic covariance matrix of Pantheon+ and SH0ES, respectively. On the other hand, ΔD is the difference between the distance of SN+ and either the distance of the host galaxies calculated from SH0ES or the distance calculated by the predicted model. In this study, the Pantheon+ data will be used with the SH0ES prior and will be referred to as SN+SH0ES.

- **Baryon Acoustic Oscillation (BAO):** For the BAO data, the ratio $\frac{r_s}{D_V}$ serves as a “standard ruler,” where r_s represents the comoving sound horizon at the baryon drag epoch, and D_V denotes the effective distance derived from D_A . The angular diameter distance D_A and the Hubble parameter H are connected via the equation below:

$$D_V(z) = \left[(1+z^2) D_A(a)^2 \frac{z}{H(z)} \right]^{\frac{1}{3}}. \quad (17)$$

This dataset uses data from large-scale surveys such as the Sloan Digital Sky Survey (SDSS) [39] of DR10 and DR11 [40, 41], the Dark Energy Survey (DES) [42] and the Baryon Oscillation Spectroscopic Survey (BOSS) DR10 [43, 44]. The χ^2 function of the BAO dataset is as follows [28],

$$\chi_{BAO}^2 = \sum_i \frac{[r_{BAO,i}^{obs} - r_{BAO,i}^{th}]^2}{\sigma_i^2}, \quad (18)$$

where r_{BAO} is equivalent to $\frac{r_s(z_d)}{D_V}$ and σ_i represents the uncertainty in the measurements for each data point i . From now on, this data will be known as the BAO data.

- **Dark Energy Spectroscopic Instrument (DESI):** The DESI 2024 dataset represents 2D BAO data collected by using the Dark Energy Spectroscopic Instrument. It includes information from bright galaxies, a combination of luminous red galaxies (LRGs) and emission-line galaxies (ELGs), quasars,

and the Lyman- α Forest [45]. LRGs are older, massive galaxies, while ELGs are younger, actively star-forming galaxies. Quasars are luminous objects fueled by supermassive black holes at the centres of galaxies, and the Lyman- α Forest consists of absorption features in the spectra of distant quasars, which serve as tools for probing the intergalactic medium [46]. From this data, DESI calculates the values of:

$$\frac{D_H(z)}{r_d} = \frac{da(1+z)}{r_d}, \quad (19)$$

$$\frac{D_M(z)}{r_d} = \frac{c}{H(z)r_d}, \quad (20)$$

$$\frac{D_V(z)}{r_d} = \frac{(zD_M(z)^2 D_H(z))^{\frac{1}{3}}}{r_d}, \quad (21)$$

where r_d is the sound horizon at the drag epoch, D_H refers to the Hubble distance, da is the angular distance, D_M represents the comoving angular diameter distance, and D_V is the volume-averaged distance. The DESI dataset determines the likelihood function [45] with the equation:

$$\chi^2 = (\mathbf{p}_A - \mathbf{p}_B)^T (Cov_A + Cov_B)^{-1} (\mathbf{p}_A - \mathbf{p}_B), \quad (22)$$

where \mathbf{p}_A and \mathbf{p}_B refer to the Ω_m and $r_d h$ parameters vectors while Cov_A and Cov_B are 2×2 covariances. This dataset will be referred to as the DESI data [45].

For the analysis of the different cosmological scenarios influenced by the dynamical dark energy models, MontePython [47, 48] software was used in conjunction with the software package CLASS [49, 50]. CLASS is widely used in the research community for its ability to derive constraints on cosmological parameters from data analysis, while MontePython handles the Monte Carlo Markov Chains (MCMC). The packages make use of a convergence diagnostic method developed by Gelman and Rubin and support the chosen likelihoods of Planck, Pantheon+SH0ES, Cosmic Chronometers, BAO and DESI. The software package GetDist [51] was used for the plotting of the triangular plots. The six parameters of the Λ CDM model were adopted, which include: the physical energy density in baryons ω_b ; the physical energy density in CDM ω_{cdm} ; the spectral index of the primordial scalar perturbations n_s ; the amplitude of the primordial scalar perturbations $\ln(10^{10} A_s)$; the optical depth to reionization τ_{reio} ; and the angular size of the sound horizon $100\theta_s$. Additionally, the parameters relating to the dark energy models of w_0 for the w_0 CDM model or w_0 and w_a for the other models were included.

4. w CDM CONSTRAINT ANALYSIS

In this section, the key observational findings derived from all the cosmological models analysed using various datasets are presented. The primary focus is on the estimation of H_0 , as influenced by the underlying cosmological models driven by different dark energy parameterisations. However, the σ_8 parameter will also be analysed for the different models. For a clearer understanding of H_0 and σ_8 estimations across different datasets and models, we refer to the posterior plots and the tables containing the values obtained for each parameter.

4.1. Constant parameterisation:

A combined analysis was carried out for the w_0 CDM model, with the main observational constraints summarised in Table S1 - Table S4 where each table shows the best-fit, mean and 1σ deviation from the mean value for the different data combinations that were taken for the six Λ CDM parameters and for $w_0, w_0 CDM$, H_0 , and σ_8 . Table S1 show the results of the constant parameterisation when combinations of late-time data was used, Table S2 show the parameters' values when PR3 and PR4, separately were used, while Table S3 and Table S4 show the values when PR3 and PR4 were used with CC, and SN+SH0ES and when PR3 and PR4 were used in conjunction to CC, SN+SH0ES, and DESI, respectively.

Additionally, Fig. 1 illustrates the 1σ and 2σ confidence-level contour plots and the marginalised 1-dimensional posterior distributions for various combinations of late-time data, of the constant model parameters and the derived parameters. The figure shows that the older BAO data favours the results obtained by

Parameters	CC + SN+SH0ES		CC + SN+SH0ES BAO		CC + SN+SH0ES DESI	
	Best-fit	Mean	Best-fit	Mean	Best-fit	Mean
Sampled Parameters						
Ω_m	0.270	$0.270^{+0.052}_{-0.042}$	0.273	$0.274^{+0.013}_{-0.043}$	0.317	$0.318^{+0.011}_{-0.012}$
$w_{0,w0CDM}$	-0.88	$-0.89^{+0.12}_{-0.10}$	-0.888	$-0.894^{+0.043}_{-0.040}$	-1.054	$-1.056^{+0.036}_{-0.034}$
Derived Parameters						
H_0 / km s ⁻¹ Mpc ⁻¹ ..	72.35	72.34 ± 0.88	72.35	$72.33^{+0.86}_{-0.87}$	71.43	$71.46^{+0.81}_{-0.82}$
χ^2 Statistics						
χ^2_{min}	1309		1322		1332	
ΔAIC	0.91		-4.38		-0.65	
ΔBIC	6.37		1.09		4.81	

TABLE S1. The values of the constant model using different late-time data combinations: CC and SN+SH0ES; CC, SN+SH0ES, and BAO; and CC, SN+SH0ES, and DESI.

Parameters	PR3		PR4	
	Best-fit	Mean	Best-fit	Mean
Sampled Parameters				
ω_b	0.02247	$0.02239^{+0.00015}_{-0.00016}$	0.02229	0.02224 ± 0.00013
ω_{cdm}	0.1191	0.1197 ± 0.0014	0.1184	0.1188 ± 0.0012
$100\theta_s$	1.0420	$1.0419^{+0.00030}_{-0.00031}$	1.0418	1.0418 ± 0.00025
$\ln(10^{10}A_s)$	3.054	$3.042^{+0.016}_{-0.017}$	3.0366	3.0383 ± 0.014
n_s	0.9654	$0.9651^{+0.0043}_{-0.0045}$	0.9691	$0.9674^{+0.0042}_{-0.0041}$
τ_{reio}	0.0574	$0.0592^{+0.0078}_{-0.0087}$	0.0593	$0.0576^{+0.0062}_{-0.0063}$
$w_{0,w0CDM}$	-2.30	$-1.92^{+0.29}_{-0.48}$	-1.24	$-1.14^{+0.20}_{-0.26}$
Derived Parameters				
H_0 / km s ⁻¹ Mpc ⁻¹ ..	115.45	$100.16^{+20.00}_{-10.00}$	75.41	$72.00^{+8.00}_{-7.00}$
σ_8	1.17	$1.07^{+0.14}_{-0.06}$	0.871	$0.840^{+0.071}_{-0.060}$
χ^2 Statistics				
χ^2_{min}	2766		30570	
ΔAIC	-4.40		1.80	
ΔBIC	10.04		9.90	

TABLE S2. The values of the constant model obtained from the chosen simulations when only Planck data, PR3 and PR4 were used.

the CC and SN+SH0ES data, as the 1D curves overlap and the model shows a preference for a quintessence-like Universe. On the other hand, the DESI data pushes the H_0 , and w_0 values to lower values to phantom energy. The Ω_m parameter shows the difference between the DESI data set and the BAO data set. The figure shows that when DESI was added, the constant model had a higher value of Ω_m than when BAO data was used or when only CC+SN+SH0ES was considered. The DESI data shows that it constrains the model better, as the posteriors were the smallest out of the three. Now, moving on to Fig. 2, which is similar to the previous plot, shows the 1D marginalised posteriors and the 1σ and 2σ confidence levels in the 2D posteriors of the constant model when using the early time data of PR3 and PR4 for comparison. The figure

Parameters	PR3		PR4	
	CC + SN+SH0ES		CC + SN+SH0ES	
	Best-fit	Mean	Best-fit	Mean
Sampled Parameters				
ω_b	0.02251	0.02252 ± 0.00015	0.02224	0.02235 ± 0.00012
ω_{cdm}	0.1179	0.1185 ± 0.0013	0.11833	0.1176 ± 0.0011
$100\theta_s$	1.04210	1.04207 ± 0.00029	1.04180	1.0420 ± 0.0039
$\ln(10^{10} A_s)$	3.049	$3.050^{+0.014}_{-0.015}$	3.041	3.041 ± 0.014
n_s	0.9705	$0.9693^{+0.0042}_{-0.0047}$	0.9684	0.9703 ± 0.0039
τ_{reio}	0.0577	$0.0583^{+0.0075}_{-0.0073}$	0.0616	0.0594 ± 0.0062
$w_{0,w0CDM}$	-1.034	$-1.053^{+0.026}_{-0.025}$	-1.062	-1.049 ± 0.024
Derived Parameters				
H_0 / km s $^{-1}$ Mpc $^{-1}$..	69.40	$69.80^{+0.67}_{-0.70}$	69.74	69.76 ± 0.66
σ_8	0.816	0.823 ± 0.011	0.823	$0.818^{+0.011}_{-0.010}$
χ^2 Statistics				
χ^2_{min}		4107		31900
ΔAIC		-4.44		-1.40
ΔBIC		3.60		6.96

TABLE S3. The values of the constant model obtained from the two Planck data when CC and SN+SH0ES data were added: PR3+CC+SN+SH0ES; and PR4+CC+SN+SH0ES.

Parameters	PR3		PR4	
	CC + SN+SH0ES + DESI		CC + SN+SH0ES + DESI	
	Best-fit	Mean	Best-fit	Mean
Sampled Parameters				
ω_b	0.02258	0.02256 ± 0.00014	0.02245	0.02236 ± 0.00012
ω_{cdm}	0.1176	$0.1180^{+0.0011}_{-0.0010}$	0.11704	$0.11742^{+0.00092}_{-0.00090}$
$100\theta_s$	1.04220	1.04210 ± 0.00029	1.04200	$1.04200^{+0.00024}_{-0.00025}$
$\ln(10^{10} A_s)$	3.056	$3.054^{+0.015}_{-0.020}$	3.041	3.040 ± 0.015
n_s	0.9747	$0.97033^{+0.0040}_{-0.0039}$	0.9709	$0.9707^{+0.0035}_{-0.0036}$
τ_{reio}	0.0623	$0.0606^{+0.0073}_{-0.0099}$	0.0614	$0.0597^{+0.0063}_{-0.0067}$
$w_{0,w0CDM}$	-1.038	$-1.049^{+0.026}_{-0.024}$	-1.043	-1.046 ± 0.024
Derived Parameters				
H_0 / km s $^{-1}$ Mpc $^{-1}$..	69.70	69.86 ± 0.61	69.89	$69.76^{+0.63}_{-0.62}$
σ_8	0.820	$0.823^{+0.011}_{-0.013}$	0.813	0.816 ± 0.010
χ^2 Statistics				
χ^2_{min}		4122		31920
ΔAIC		-3.24		-1.00
ΔBIC		4.80		7.36

TABLE S4. The values of the constant model obtained from the two Planck data when DESI was added to the CC and SN+SH0ES data: PR3+CC+SN+SH0ES+DESI; and PR4+CC+SN+SH0ES+DESI.

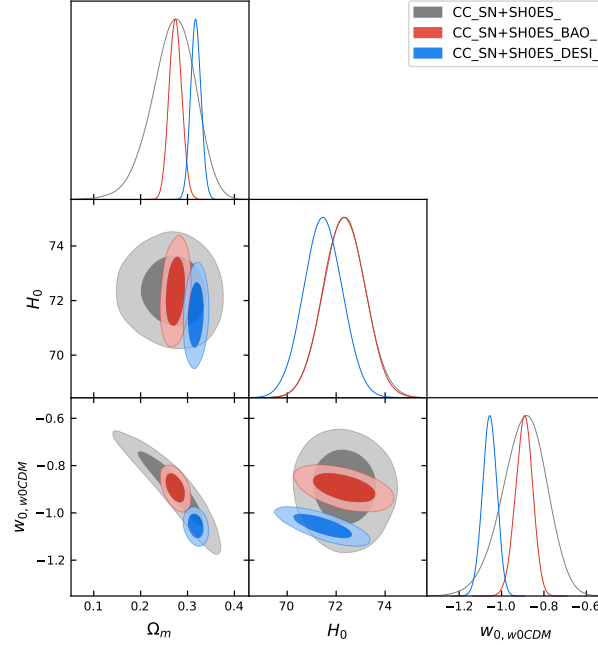


FIG. 1. The graph presents three overlapping corner plots of the constant model, utilising only late-time data. The grey plot represents CC + SN+SH0ES, the red plot corresponds to CC + SN+SH0ES + BAO, and the blue plot illustrates CC + SN+SH0ES + DESI.

shows uncertainty with regard to the exact value of w_0 , H_0 and σ_8 in both datasets as degeneracies, but it is seen more with PR4. When PR3 was taken, the constant model favours phantom energy and produced higher values of H_0 and σ_8 , which go beyond the expected values of past research [2, 24, 26, 46]. Differences between the two Planck datasets can be seen with regard to the six Λ CDM parameters. The newer Planck data produced higher values of τ_{reio} , and n_s , while lower values of w_b , and w_{cdm} , than the previously released data set. These differences in values show the differences between the two Planck data sets. From the 2D posteriors, it can be concluded that the constant model obtained the smallest posteriors when the PR4 model was taken, showing that the newer Planck data has less uncertainty regarding the possible values of each parameter. Similarly, Fig. 3 shows the 1D marginalised posteriors and the 1σ and 2σ confidence levels in the diagonal and off-diagonal panels, respectively, of the constant model when combining early-time with late-time data. Any degeneracies that were seen in the previous plot, when only early-time data was taken, were removed as soon as late-time data was added to the constant model. The constant model shows no uncertainties with the parameters $w_0, w_{0\text{CDM}}$ and H_0 as the constant model achieved the same 1D curve for each data combination. The figure illustrates how the addition of the DESI data did not affect the results of the model except for constraining the 2D posteriors better. In fact, the constant model obtained the smallest 2D posteriors when PR4+CC+SN+SH0ES+DESI data combination was used, indicating that this model constrained the parameters the best when considering this data combination. The plot continues to show that the constant model favours a phantom Universe.

In summary, the constant model favours a phantom Universe, and when using CC+SN+SH0ES and PR4, the model is 1σ away from the Λ CDM model. Also, both DESI and PR4 show to be better data sets than their predecessors as they constrain the parameters better.

4.2. Quadratic parameterisation:

Similar to the constant parametrisation, the quadratic model underwent a series of analyses, with the results summarised in Table S5, Table S6, Table S7, and Table S8, showcasing the observational constraints, by showing the best-fit values, the mean values and the 1σ uncertainty of the six Λ CDM parameters, w_0, w_{JBP} , w_a, w_{JBP} , H_0 and σ_8 parameters. Table S5 shows the values of the quadratic model when combinations of

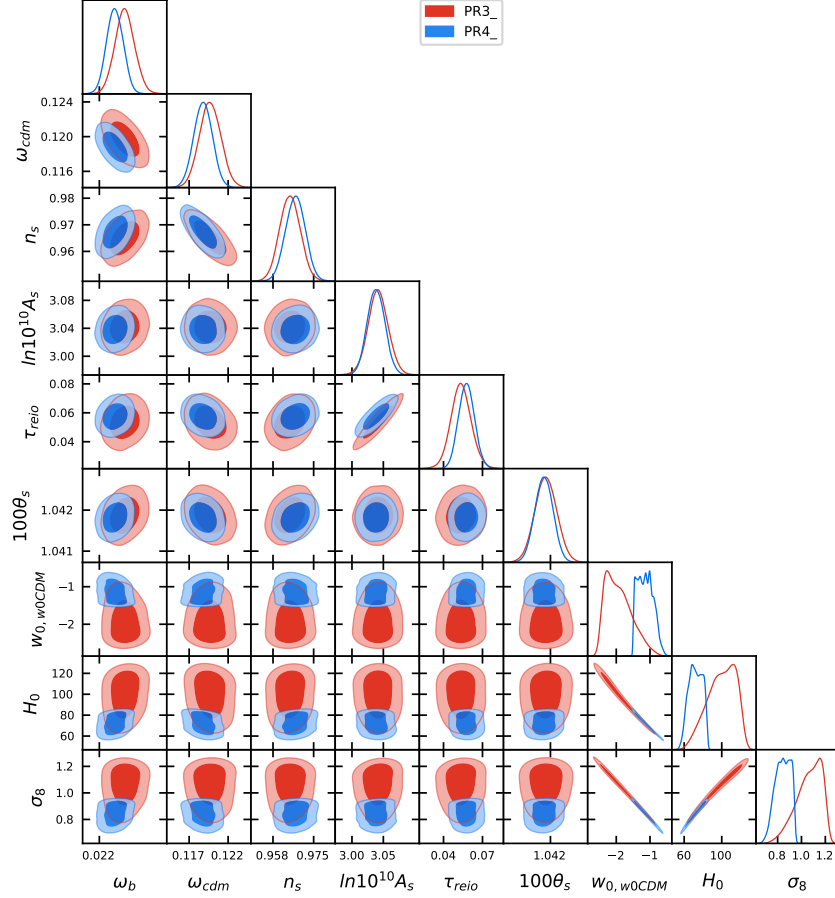


FIG. 2. The graph shows the w_0 CDM model, with PR3 represented in red and PR4 in blue.

late-time data were taken, Table S6 show the quadratic model when Planck data was used, Table S7 shows the model when Planck data was used with CC, and SN+SH0ES data was considered, and Table S8 shows the values when Planck data with CC, SN+SH0ES, and DESI were taken. Fig. 4 displays the 1σ and 2σ confidence levels posteriors in the off-diagonal panels and the 1D marginalised posteriors in the diagonal panels of the quadratic model when only late-time data combinations were considered. The BAO data with respect to the quadratic parameterisation did not have any effect on the H_0 parameter, while the DESI data has lowered the value of this parameter. The BAO data did have a slight effect on the $w_{0,JBP}$ and $w_{a,JBP}$ parameters, shifting them to slightly lower and slightly higher values, respectively. On the other hand, the DESI data had the opposite effect on the $w_{0,JBP}$ and the $w_{a,JBP}$ parameters. When looking at the Ω_m parameter, the quadratic model obtained a higher value when DESI was included than when DESI was not. This further highlights the differences between DESI and BAO data sets. From the off-diagonal panels, it can be seen that when the DESI data was included, this parameterisation had constrained the parameters the best out of the three data combinations. From Table S5 it is concluded that the quadratic model favours a quintessence Universe at current times, but at high redshifts the preference changes to a phantom Universe. Fig. 5 presents the diagonal and off-diagonal panels representing the 1D marginalised posteriors and the 1σ and 2σ confidence levels, respectively, of the quadratic parameterisation when the two Planck data were taken separately. From the figure, degeneracies in the quadratic parameterisation, can be spotted with the $w_{0,JBP}$, $w_{a,JBP}$, H_0 , and σ_8 parameters when the PR3 data was considered, showing other possible values that the parameters can obtain apart from the highest peak shown in the 1D posteriors. Differences between the datasets can be seen when one looks at the six Λ CDM parameters, as PR4 obtained lower values of w_{cdm} , w_b , and $\ln 10^{10} A_s$ while higher values of n_s , and τ_{reio} when compared to PR3. This model seems to agree with the most probable value of $w_{a,JBP}$, H_0 , and σ_8 when the two Planck data sets

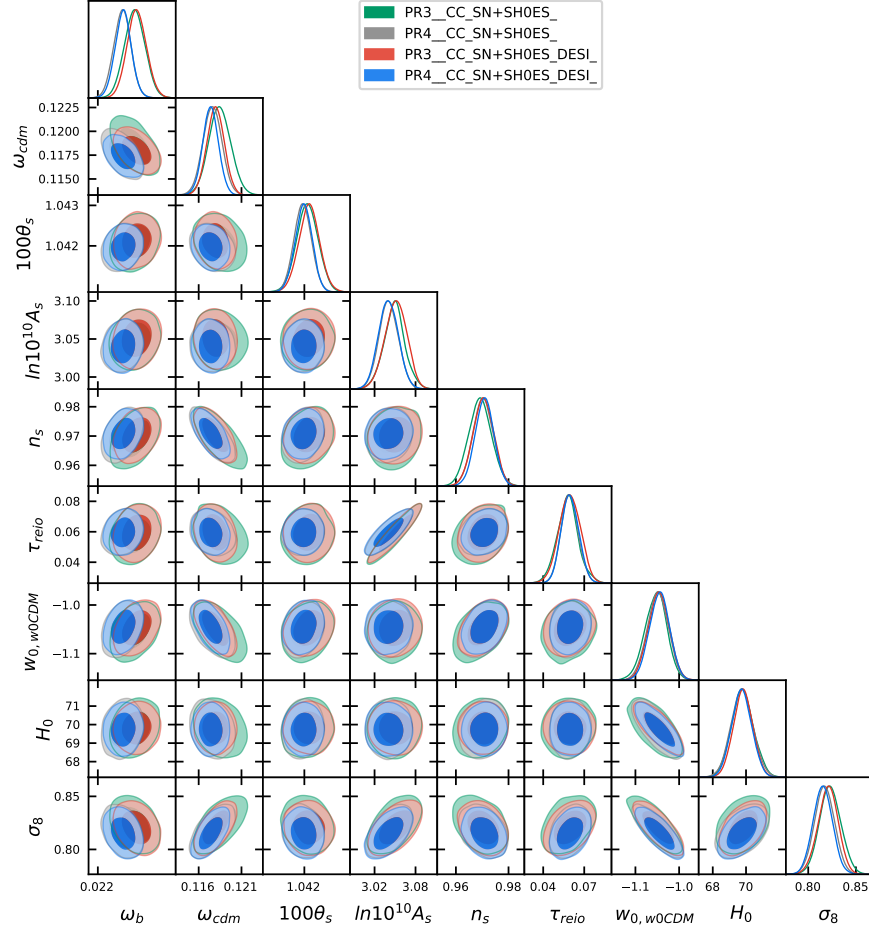


FIG. 3. The graph depicts the constant model under different data combinations. The green plot represents CC + SN+SH0ES with PR3, while the grey plot corresponds to PR4. When CC + SN+SH0ES + DESI is used, the red plot depicts PR3, and the blue plot represents PR4.

Parameters	CC + SN+SH0ES		CC + SN+SH0ES BAO		CC + SN+SH0ES DESI	
	Best-fit	Mean	Best-fit	Mean	Best-fit	Mean
Sampled Parameters						
Ω_m	0.225	$0.242^{+0.098}_{-0.063}$	0.270	$0.273^{+0.015}_{-0.016}$	0.322	0.324 ± 0.011
$w_{0,JBP}$	-0.89	$-0.90^{+0.12}_{-0.10}$	-0.93	$-0.91^{+0.10}_{-0.11}$	-0.83	$-0.84^{+0.11}_{-0.09}$
$w_{a,JBP}$	0.73	$0.28^{+1.40}_{-0.85}$	0.31	$0.15^{+0.96}_{-0.85}$	-1.71	$-1.64^{+0.64}_{-0.82}$
Derived Parameters						
H_0 / $\text{km s}^{-1}\text{Mpc}^{-1}$..	72.47	72.40 ± 0.89	72.29	$72.36^{+0.87}_{-0.88}$	71.49	$71.48^{+0.80}_{-0.81}$
χ^2 Statistics						
χ^2_{min}	1309		1322		1327	
ΔAIC	0.61		-0.38		-3.71	
ΔBIC	13.52		1.09		7.22	

TABLE S5. The values of the JBP model when using only late-time data.

Parameters	PR3		PR4	
	Best-fit	Mean	Best-fit	Mean
Sampled Parameters				
ω_b	0.02244	$0.02238^{+0.00015}_{-0.00016}$	0.02231	0.02226 ± 0.00013
ω_{cdm}	0.1177	0.1199 ± 0.0014	0.11837	0.11870 ± 0.00012
$100\theta_s$	1.04180	$1.04190^{+0.00031}_{-0.00030}$	1.04190	$1.04180^{+0.00025}_{-0.00025}$
$\ln(10^{10}A_s)$	3.044	3.045 ± 0.016	3.047	$3.049^{+0.014}_{-0.015}$
n_s	0.9712	0.9654 ± 0.0046	0.9690	0.9676 ± 0.0041
τ_{reio}	0.0580	$0.0543^{+0.0074}_{-0.0081}$	0.0623	$0.0578^{+0.0060}_{-0.0066}$
$w_{0,JBP}$	-0.807	$-1.235^{+0.004}_{-0.266}$	-1.05	$-1.15^{+0.11}_{-0.35}$
$w_{a,JBP}$	-1.07	$-0.99^{+2.49}_{-0.16}$	-1.00	$0.11^{+0.47}_{-0.87}$
Derived Parameters				
H_0 / km s ⁻¹ Mpc ⁻¹ ..	11078	$79.03^{+4.83}_{-9.14}$	74.29	$73.03^{+8.64}_{-7.52}$
σ_8	1.134	$0.911^{+0.044}_{-0.078}$	0.867	$0.851^{+0.079}_{-0.059}$
χ^2 Statistics				
χ^2_{min}		2767		30570
ΔAIC		-2.08		3.60
ΔBIC		14.00		20.32

TABLE S6. The values of the JBP model using the two Planck data sets: PR3 or PR4.

Parameters	PR3		PR4	
	CC + SN+SH0ES		CC + SN+SH0ES	
	Best-fit	Mean	Best-fit	Mean
Sampled Parameters				
ω_b	0.02250	$0.02248^{+0.00014}_{-0.00015}$	0.02233	$0.02232^{+0.00013}_{-0.00012}$
ω_{cdm}	0.1192	$0.1191^{+0.0013}_{-0.0012}$	0.1182	$0.1180^{+0.0011}_{-0.0012}$
$100\theta_s$	1.04190	$1.04200^{+0.00028}_{-0.00031}$	1.04200	1.04190 ± 0.00025
$\ln(10^{10}A_s)$	3.049	$3.046^{+0.016}_{-0.018}$	3.025	$3.040^{+0.015}_{-0.014}$
n_s	0.9653	0.9676 ± 0.0044	0.9670	0.9693 ± 0.0039
τ_{reio}	0.0550	$0.0558^{+0.0078}_{-0.0084}$	0.0540	$0.0590^{+0.0063}_{-0.0065}$
$w_{0,JBP}$	-0.706	$-0.790^{+0.090}_{-0.021}$	-0.802	$-0.858^{+0.058}_{-0.013}$
$w_{a,JBP}$	-2.37	$-1.84^{+0.31}_{-0.58}$	-1.63	$-1.34^{+0.25}_{-0.42}$
Derived Parameters				
H_0 / km s ⁻¹ Mpc ⁻¹ ..	70.10	$70.24^{+0.68}_{-0.69}$	69.81	70.18 ± 0.68
σ_8	0.834	0.833 ± 0.012	0.817	0.826 ± 0.011
χ^2 Statistics				
χ^2_{min}		4098		31900
ΔAIC		-11.36		-8.40
ΔBIC		4.72		8.32

TABLE S7. The values obtained from the JBP model when using PR3 and PR4 with CC and SN+SH0ES data.

Parameters	PR3		PR4	
	CC + SN+SH0ES + DESI		CC + SN+SH0ES + DESI	
	Best-fit	Mean	Best-fit	Mean
Sampled Parameters				
ω_b	0.02262	0.02247 ± 0.00014	0.02238	$0.02232^{+0.00012}_{-0.00011}$
ω_{cdm}	0.1188	0.1191 ± 0.0011	0.11825	$0.11808^{+0.00095}_{-0.00097}$
$100\theta_s$	1.04190	$1.04190^{+0.00029}_{-0.00030}$	1.04190	$1.04190^{+0.00024}_{-0.00023}$
$\ln(10^{10} A_s)$	3.044	3.046 ± 0.016	3.034	3.039 ± 0.014
n_s	0.9697	$0.9674^{+0.0041}_{-0.0040}$	0.9690	$0.9692^{+0.0037}_{-0.0036}$
τ_{reio}	0.0528	$0.0559^{+0.0076}_{-0.0081}$	0.0572	$0.0585^{+0.0060}_{-0.0064}$
$w_{0,JBP}$	-0.78	$-0.81^{+0.10}_{-0.04}$	-0.830	$-0.878^{+0.078}_{-0.022}$
$w_{a,JBP}$	-1.75	$-1.60^{+0.39}_{-0.58}$	-1.41	$-1.12^{+0.29}_{-0.47}$
Derived Parameters				
H_0 / km s ⁻¹ Mpc ⁻¹ ..	69.68	69.80 ± 0.59	69.67	$69.75^{+0.60}_{-0.63}$
σ_8	0.825	$0.830^{+0.012}_{-0.011}$	0.820	0.822 ± 0.010
χ^2 Statistics				
χ^2_{min}		4114		31910
ΔAIC		-9.48		-6.40
ΔBIC		6.60		10.32

TABLE S8. Values of the quadratic model obtained from PR3 + CC + SN+SH0ES + DESI and PR4 + CC + SN+SH0ES + DESI.

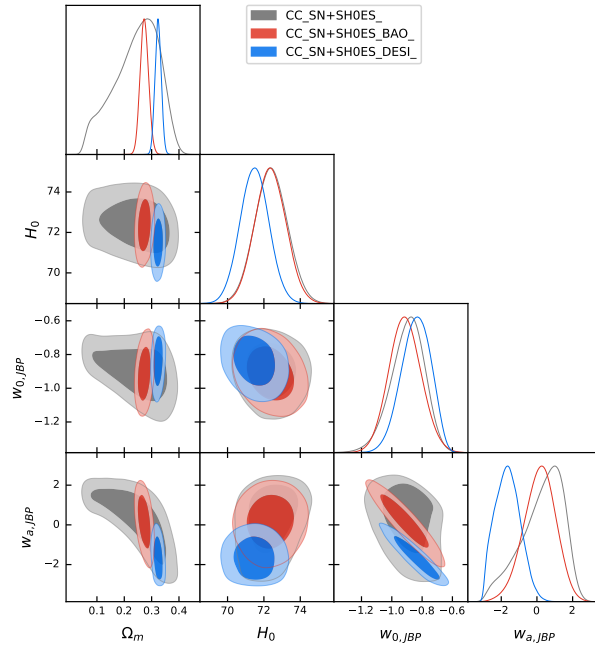


FIG. 4. A graph depicting the quadratic model when late-time data combinations were taken. The grey corner plot shows the model when CC, and SN+SH0ES data combination was considered, the red corner plot shows the model when the CC, SN+SH0ES, and BAO data combination was used, and the blue corner plot shows the parameterisation when CC, SN+SH0ES, and DESI data were taken.

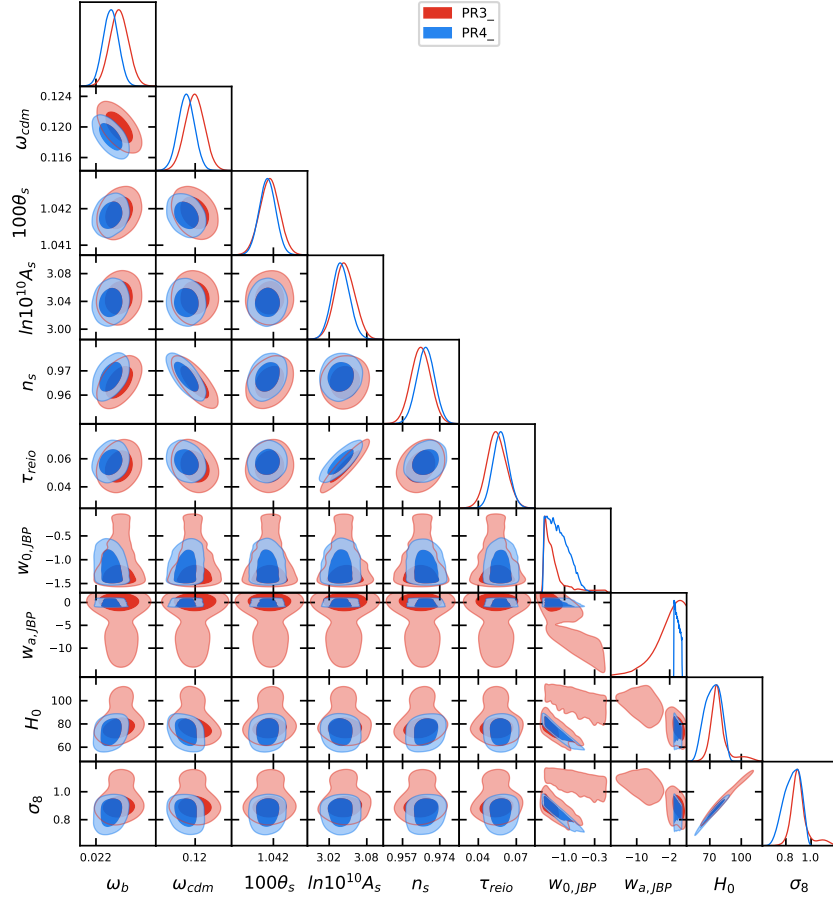


FIG. 5. A graph showing the results of the quadratic parameterisation when using PR3, shown in the red corner plot, and when considering the PR4 data set shown in the blue corner plot.

were considered. When comparing the two data sets, it can be seen that the Quadratic model constrains the parameters the best when the latest Planck data is used. When only early-time data is taken, the quadratic model suggests a phantom Universe when the PR3 or PR4 data were considered. Fig. 6 displays the 1D marginalised posteriors, and the 1σ and 2σ confidence level posteriors showcasing any correlations and anti-correlations between parameters when the quadratic parameterisation was assumed, taking combinations of early-time with late-time data. This figure shows that the quadratic model obtained slight degeneracies with the $w_{0,JBP}$ and $w_{a,JBP}$ parameters when the PR4 + CC + SN+SH0ES data combination was taken, while when the other data combinations were taken, the model did not show any degeneracies. The addition of the DESI data did not impact the model much, as it only slightly shifted the parameters to lower or higher values. Similar to when late-time data combinations, the quadratic model prefers a quintessence Universe at low redshifts, but then favours a Phantom Universe at high redshifts. The smallest posteriors were obtained through the PR4 + CC + SN+SH0ES + DESI data combination, implying that DESI and PR4 help constrain the quadratic model the best.

In conclusion, the quadratic model favours a quintessence dark energy at low redshifts, but then changes to a phantom dark energy at high redshifts when late-time data is used. When only early-time data was considered, the model favoured a phantom Universe. The model seems to perform the best when DESI and PR4 data were used, showing that they are more accurate than their predecessor.

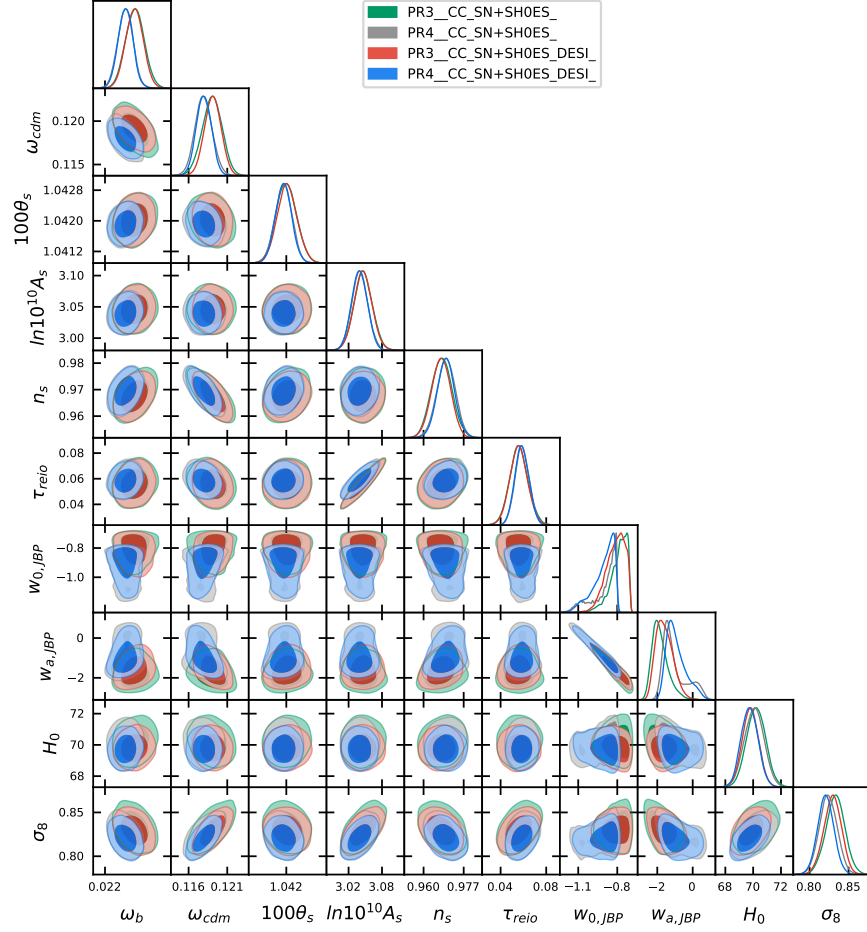


FIG. 6. A graph showing the quadratic parameterisation when combinations of early-time and late-time data were considered. The green plot shows when PR3, CC, and SN+SH0ES were taken, the grey plot depicts when PR4, CC, and SN+SH0ES were used, the red plot displays the results obtained from when PR3, CC, SN+SH0ES, and DESI were taken, and the blue plot shows when PR4, CC, SN+SH0ES, and DESI were considered.

4.3. Logarithmic parameterisation:

Following the trend of the previous two models, a combination of analyses was performed on the Logarithmic model, and in Table S9, Table S10, Table S11, and Table S12 contain the summary of the observational constraints, showcasing the values of the best-fit, the mean, and the 1σ variation for the Logarithmic model when combination of late-time, early-time and early-time with late-time data were taken. Fig. 7 depicts the 1σ and 2σ confidence-level contour plots and the marginalised 1-dimensional posterior distributions for three late-time data combinations for the Logarithmic model and possible correlations between certain parameters. The plot shows that despite there being a high certainty of the value of H_0 there is another possible value, even though it is less likely. Degeneracies are also seen with the parameter of $w_{a,GE}$ for all the late-time combinations. Similar to the w_0 CDM model, the BAO data seems to barely affect the model when added to the CC+SN+SH0ES data combination and suggests a quintessence-like Universe, while DESI did, as the Logarithmic model favoured a phantom Universe and a lower H_0 more when DESI was included. When CC + SN+SH0ES and CC + SN+SH0ES + BAO were considered, the Logarithmic model predicts a quintessence Universe at current times, but at higher red shifts, the model describes a Phantom Universe. Following the trend of the previous models, the BAO data set is in agreement with the CC+SN+SH0ES data combination when it comes to the value of the Ω_m parameter. This is not the case when the DESI data was added, as the dataset shifted the parameter to higher values. The DESI data achieved the smallest

Parameters	CC + SN+SH0ES		CC + SN+SH0ES		CC + SN+SH0ES	
			BAO		DESI	
	Best-fit	Mean	Best-fit	Mean	Best-fit	Mean
Sampled Parameters						
Ω_m	0.269	$0.300^{+0.045}_{-0.059}$	0.274	$0.291^{+0.011}_{-0.033}$	0.437	$0.354^{+0.017}_{-0.052}$
$w_{0,GE}$	-0.88	$-0.91^{+0.11}_{-0.09}$	-0.888	$-0.876^{+0.046}_{-0.042}$	-1.023	$-1.033^{+0.037}_{-0.036}$
$w_{a,GE}$	-0.014	$-0.092^{+0.063}_{-0.055}$	-0.01507	$-0.12^{+0.13}_{-0.04}$	-0.183	$-0.118^{+0.023}_{-0.072}$
Derived Parameters						
H_0 / km s ⁻¹ Mpc ⁻¹ ..	72.34	$70.50^{+3.40}_{-1.10}$	72.25	$70.73^{+2.90}_{-4.03}$	61.15	$68.24^{+4.38}_{-1.83}$
χ^2 Statistics						
χ^2_{min}		1309		1322		1329
ΔAIC		0.93		4.02		-1.86
ΔBIC		13.84		14.95		9.06

TABLE S9. The values of the Logarithmic model using different late-time data combinations: CC and SN+SH0ES; CC, SN+SH0ES, and BAO; and CC, SN+SH0ES, and DESI.

Parameters	PR3		PR4	
	Best-fit	Mean	Best-fit	Mean
Sampled Parameters				
ω_b	0.02233	$0.02238^{+0.00015}_{-0.00016}$	0.02231	0.02223 ± 0.00013
ω_{cdm}	0.1203	0.1200 ± 0.0014	0.1179	0.1188 ± 0.0012
$100\theta_s$	1.0421	1.0419 ± 0.00030	1.0418	1.0418 ± 0.00025
$\ln(10^{10} A_s)$	3.052	3.045 ± 0.016	3.034	3.039 ± 0.014
n_s	0.9659	$0.9653^{+0.0045}_{-0.0046}$	0.9681	0.9673 ± 0.0040
τ_{reio}	0.0578	$0.0544^{+0.0076}_{-0.0081}$	0.0571	0.0577 ± 0.0062
$w_{0,GE}$	-1.14	$-1.03^{+0.05}_{-0.17}$	-1.09	-0.99 ± 0.12
$w_{a,GE}$	-0.07	$-0.18^{+0.07}_{-0.11}$	-0.014	-0.077 ± 0.043
Derived Parameters				
H_0 / km s ⁻¹ Mpc ⁻¹ ..	72.54	$70.77^{+5.02}_{-2.58}$	71.15	$67.62^{+5.02}_{-3.06}$
σ_8	0.864	$0.843^{+0.046}_{-0.022}$	0.829	$0.806^{+0.046}_{-0.026}$
χ^2 Statistics				
χ^2_{min}		2770		30570
ΔAIC		1.72		3.00
ΔBIC		17.80		19.61

TABLE S10. The values of the GE model when only early-time data of PR3 and PR4 were used.

2D posteriors out of the three data combinations, showing the model constraining the parameters the best when DESI was included. Fig. 8 shows the 1D curves in the diagonal panels and the 2D posteriors in the off-diagonal panels showing the 1σ and 2σ confidence levels of the Logarithmic model when only early-time data of PR3 and PR4 were taken. Similar to the previous models, the graph shows differences between the datasets with regard to the six standard parameters. When the latest Planck data was taken, the model obtained lower values of w_{cdm} , w_b , $\ln 10^{10} A_s$, and $100\theta_s$. On the other hand, the logarithmic model produced

Parameters	PR3		PR4	
	CC + SN+SH0ES		CC + SN+SH0ES	
	Best-fit	Mean	Best-fit	Mean
Sampled Parameters				
ω_b	0.02248	0.02251 ± 0.00015	0.022426	0.02235 ± 0.00012
ω_{cdm}	0.1182	0.1186 ± 0.0013	0.11743	0.1176 ± 0.0011
$100\theta_s$	1.0419	1.04205 ± 0.00029	1.0420	1.04195 ± 0.00024
$\ln(10^{10}A_s)$	3.055	3.046 ± 0.016	3.0464	3.040 ± 0.014
n_s	0.9678	0.9688 ± 0.0043	0.9704	0.9704 ± 0.0039
τ_{reio}	0.0630	$0.0565^{+0.0074}_{-0.0082}$	0.0588	0.0593 ± 0.0063
$w_{0,GE}$	-0.932	$-0.960^{+0.034}_{-0.082}$	-0.978	$-1.004^{+0.029}_{-0.026}$
$w_{a,GE}$	-0.274	$-0.246^{+0.025}_{-0.056}$	-1.9132	$-0.149^{+0.024}_{-0.052}$
Derived Parameters				
H_0 / $\text{km s}^{-1}\text{Mpc}^{-1}$..	69.83	70.22 ± 0.68	57.22	63.60 ± 4.80
σ_8	0.828	0.830 ± 0.012	0.713	$0.767^{+0.052}_{-0.040}$
χ^2 Statistics				
χ^2_{min}		4098		31900
ΔAIC		-11.54		-6.00
ΔBIC		4.54		10.72

TABLE S11. The values of the logarithmic model when using PR3 and PR4 with CC and SN+SH0ES data: PR3+CC+SN+SH0ES; and PR4+CC+SN+SH0ES.

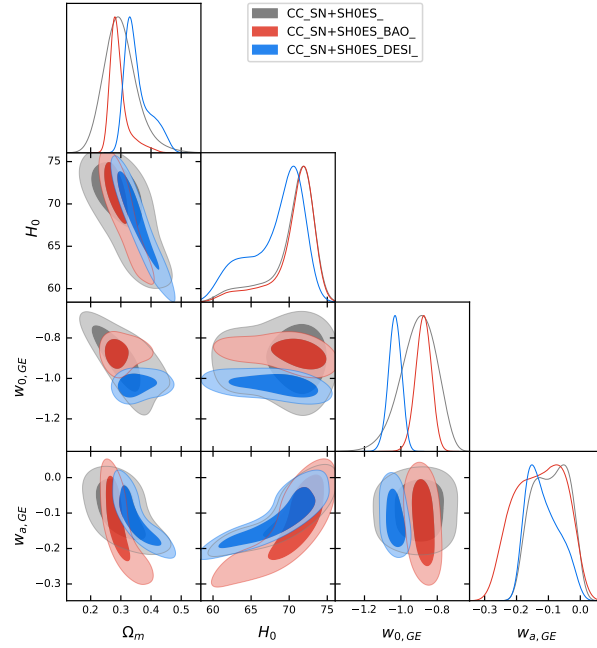


FIG. 7. The graph represents the Logarithmic model using only late-time data. The grey plot corresponds to CC + SN+SH0ES, the red plot illustrates CC + SN+SH0ES + BAO, and the blue plot depicts CC + SN+SH0ES + DESI.

Parameters	PR3		PR4	
	CC + SN+SH0ES + DESI		CC + SN+SH0ES + DESI	
	Best-fit	Mean	Best-fit	Mean
Sampled Parameters				
ω_b	0.02248	$0.02251^{+0.00015}_{-0.00016}$	0.02237	0.02234 ± 0.00012
ω_{cdm}	0.1182	$0.1186^{+0.0013}_{-0.0014}$	0.11734	$0.11776^{+0.00091}_{-0.00096}$
$100\theta_s$	1.04190	1.04210 ± 0.00030	1.04210	1.04190 ± 0.00024
$\ln(10^{10} A_s)$	3.055	3.048 ± 0.016	3.025	$3.041^{+0.015}_{-0.014}$
n_s	0.9678	$0.9688^{+0.0044}_{-0.0045}$	0.9707	0.9700 ± 0.0035
τ_{reio}	0.0622	$0.0574^{+0.0078}_{-0.0081}$	0.0525	$0.0592^{+0.0059}_{-0.0069}$
$w_{0,GE}$	-0.932	$-0.970^{+0.034}_{-0.030}$	-0.979	$-1.000^{+0.028}_{-0.025}$
$w_{a,GE}$	-0.273	$-0.245^{+0.011}_{-0.055}$	-0.195	$-0.146^{+0.013}_{-0.054}$
Derived Parameters				
H_0 / km s ⁻¹ Mpc ⁻¹ ..	69.83	$70.20^{+0.66}_{-0.68}$	56.17	$64.10^{+5.80}_{-3.90}$
σ_8	0.828	0.830 ± 0.012	0.696	$0.773^{0.049}_{-0.032}$
χ^2 Statistics				
χ^2_{min}		4098		31910
ΔAIC		-25.52		-4.60
ΔBIC		-9.44		12.12

TABLE S12. Values of the GE model obtained from the two Planck data with CC, SN+SH0ES and DESI data: PR3+CC+SN+SH0ES+DESI; and PR4+CC+SN+SH0ES+DESI.

higher values of n_s , and τ_{reio} when PR4 was considered as opposed to when PR3 was taken. The figure shows that when the Logarithmic model was considered, the model had degeneracies with obtaining the values of $w_{0,GE}$, $w_{a,GE}$, and H_0 when PR3 was taken and $w_{a,GE}$ when PR4 was included, as degeneracies can be seen. When PR3 was taken, this model seems to favour a phantom Universe, while this was not the case when PR4 was considered, as it suggests a quintessence dark energy at current time, but then changes to a phantom Universe at higher redshifts. Unlike in the previous models, the Logarithmic parametrisation obtained smaller posteriors with the six Λ CDM parameters and $w_{a,GE}$ parameter when PR4 was used, but obtained smaller posteriors with $w_{0,GE}$, H_0 , and σ_8 when PR3 was used. Fig. 9 depicts the 1D marginalised posteriors and the 2D posteriors showing the 1σ and 2σ confidence levels, of the Logarithmic model when combinations of early-time with late-time were taken. The figure demonstrates that the addition of the late-time data was enough to remove any degeneracies with the parameter $w_{0,GE}$ that were seen in the previous graph. It is also seen that when PR3 was considered, the Logarithmic model had no degeneracies with any of the parameters. This is not the case for when PR4 was taken, as degeneracies with the H_0 and σ_8 parameters are found. This figure also shows that the addition of the DESI data did not affect this model, as the results of the 1D curves obtained from using PR4+CC+SN+SH0ES data combination overlap nearly perfectly with the results retrieved from taking PR4+CC+SN+SH0ES+DESI data combination, and the same occurred when PR3 was used instead of the newer Planck data. Unlike when only Planck data was considered, when late-time data was added, the Logarithmic parameterisation shows a preference towards a quintessence-like Universe at current times. However, as the redshift increases, the Logarithmic model prefers a phantom Universe. It is important to note that the Logarithmic model obtained a higher value of σ_8 than what was found in past research [2, 26]. From this figure, it can be noted that the Logarithmic parameterisation achieves the smallest 2D posteriors PR4+CC+SN+SH0ES+DESI data combination for the six Λ CDM parameters and for the $w_{0,GE}$ parameter, while for the other parameters the logarithmic model obtained the smallest 2D posteriors when PR3+CC+SN+SH0ES+DESI data combination was used. In conclusion, the Logarithmic model only obtained values of $w_{0,GE}$ and $w_{a,GE}$ that are 1σ away from the standard model when

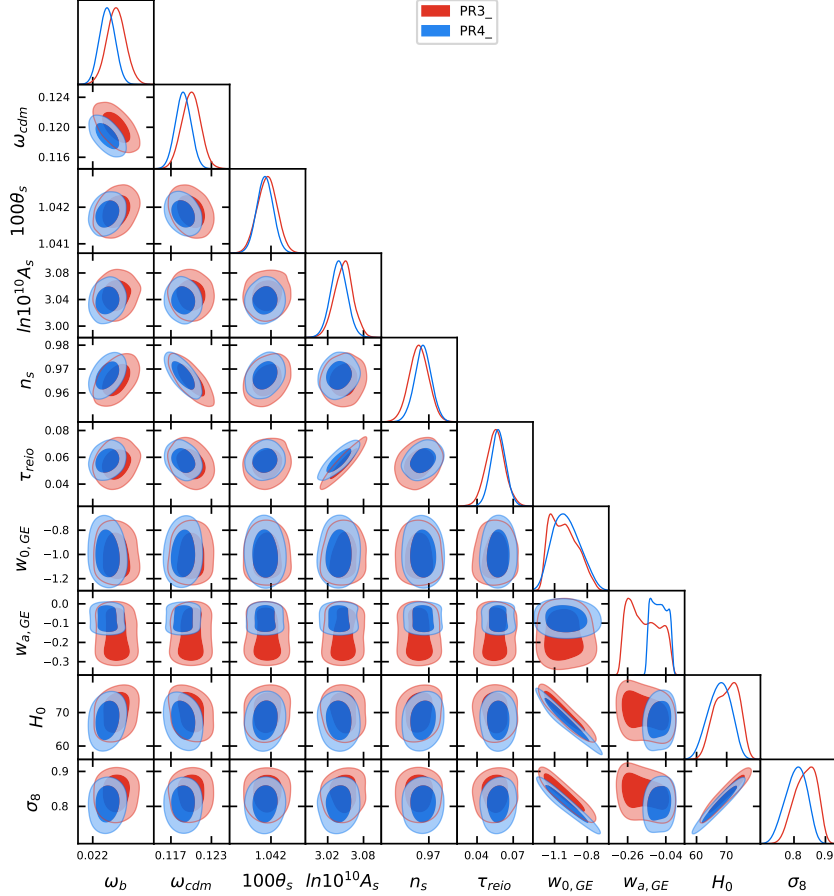


FIG. 8. The Logarithmic parameterisation is depicted using observational data, with PR4 represented in the blue corner plot and PR3 shown in the red corner plot.

PR3+CC+SN+SH0ES data combination was taken. The Logarithmic model opts for a phantom Universe when PR3 by itself was considered, and when PR4 with late-time data combinations were taken. Generally, in most data combinations, the Logarithmic parameterisation model favours a quintessence dark energy at low redshifts and then favours a phantom dark energy at high redshifts. The DESI data has been shown to be a better dataset than the BAO data, as it constrained the parameters better when the Logarithmic parameterisation was assumed. On the other hand, unlike in the previous parameterisation models, the PR4 data was a better data set when constraining the six Λ CDM parameters and the $w_{0,GE}$ parameter. However, when it came to the parameters of $w_{a,GE}$, H_0 , and σ_8 , the previously released Planck data performed better than the newer Planck data.

4.4. Oscillatory parameterisation:

The analysis of the Oscillatory parameterisation was conducted, following the trend of previous models, Table S13-Table S16 present the results achieved from the Oscillatory model showing the best-fit values, the mean values, and the 1σ deviation, when using the same data combinations as used in the previous models.

In Fig. 10 - Fig. 12 show the marginalised 1-dimensional posteriors in the diagonal panels and the 2-dimensional posteriors showcasing the 1σ and 2σ confidence levels contour plots. Fig. 10 shows the results produced by the Oscillatory parameterisation when combinations of late-time data are taken. When the CC and SN+SH0ES data combination was taken, the Oscillatory parameterisation produced a degeneracy concerning the $w_{a,OSCILL}$ parameter, which is not seen when the other data combinations were used. Apart

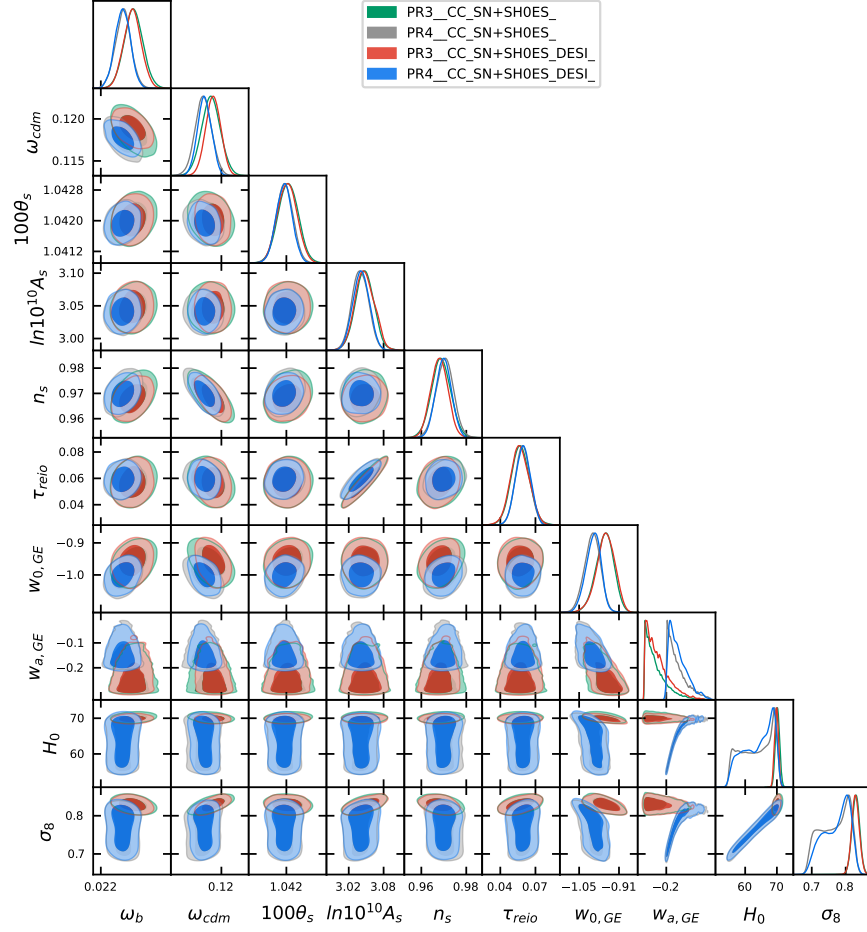


FIG. 9. The graph shows the logarithmic model using late-time data. The green plot represents the model with CC and SN+SH0ES alongside PR3, while the grey plot corresponds to PR4. When DESI is incorporated into both data combinations, the red plot depicts PR3 + CC + SN+SH0ES + DESI, and the blue plot represents PR4 + CC + SN+SH0ES + DESI.

from constraining the parameters better, the DESI data affected this model by shifting the parameter $w_{a,OSCILL}$ to higher values and the parameters $w_{0,OSCILL}$, and H_0 to lower values. On the other hand, the BAO data only constrained the parameters more, but it did not shift the parameters $w_{0,OSCILL}$, $w_{a,OSCILL}$, and H_0 to higher or lower values. As seen in the previous models, the DESI data influenced the Oscillatory parameterisation to obtain lower values of Ω_m and higher values of H_0 as opposed to when the BAO data was used. This model prefers a quintessence Universe at low redshifts, then changes preference to a Phantom Universe at high redshifts. From the 2D posteriors, it can be seen that the oscillatory model produced the smallest posteriors when the DESI data was included. This indicates that the DESI data is more accurate than the BAO data. Fig. 11 demonstrates the results of the Oscillatory model when Planck data by itself is incorporated. A complete degeneracy with the σ_8 parameter is seen in this model when the latest Planck data was used. The Oscillatory parameterisation did not have a complete degeneracy when PR3 was considered. Degeneracies are also seen with the parameters of $w_{0,OSCILL}$, and $w_{a,OSCILL}$ when PR3 was taken, while the Oscillatory model had a degeneracy with the parameter $w_{a,OSCILL}$ when PR4 was considered. The Oscillatory parameterisation assumes a phantom Universe when only Planck data was taken. The values of H_0 and σ_8 are higher than the expected values of past research [2, 26, 45]. From the 2D posteriors, it is concluded that for the six Λ CDM parameters and the $w_{a,OSCILL}$ parameter, the oscillatory model achieved smaller posteriors with the PR4 data. As for the rest of the parameters, it can be seen that this model produced smaller posteriors when the previously released Planck data, PR3, was used. Following the trend

Parameters	CC + SN+SH0ES		CC + SN+SH0ES		CC + SN+SH0ES	
			BAO		DESI	
	Best-fit	Mean	Best-fit	Mean	Best-fit	Mean
Sampled Parameters						
Ω_m	0.232	$0.278^{+0.083}_{-0.045}$	0.272	0.276 ± 0.016	0.326	0.327 ± 0.011
$w_{0,OSCILL}$	-0.85	-0.90 ± 0.11	-0.885	$-0.880^{+0.055}_{-0.062}$	-0.914	$-0.915^{+0.062}_{-0.057}$
$w_{a,OSCILL}$	-0.44	$0.50^{+0.86}_{-1.40}$	-0.07	$-0.28^{+0.57}_{-1.00}$	1.75	$1.79^{+0.67}_{-0.65}$
Derived Parameters						
H_0 / km s ⁻¹ Mpc ⁻¹ ..	72.44	72.28 ± 0.85	72.26	72.37 ± 0.88	71.78	$71.84^{+0.79}_{-0.80}$
χ^2 Statistics						
χ^2_{min}		1309		1322		1323
ΔAIC		0.89		-2.31		-7.48
ΔBIC		13.80		8.62		3.45

TABLE S13. The values retrieved from the Oscillatory model using different late-time data combinations: CC and SN+SH0ES; CC, SN+SH0ES, and BAO; and CC, SN+SH0ES, and DESI.

Parameters	PR3		PR4	
	Best-fit	Mean	Best-fit	Mean
Sampled Parameters				
ω_b	0.02249	$0.02240^{+0.00015}_{-0.00016}$	0.02222	0.02225 ± 0.00013
ω_{cdm}	0.1191	0.1198 ± 0.0014	0.1192	0.1187 ± 0.0012
$100\theta_s$	1.04170	1.04190 ± 0.00030	1.04180	1.04180 ± 0.00025
$\ln(10^{10} A_s)$	3.040	3.046 ± 0.018	3.036	$3.038^{+0.014}_{-0.015}$
n_s	0.9678	$0.9658^{+0.0044}_{-0.0046}$	0.9694	$0.9677^{+0.0041}_{-0.00040}$
τ_{reio}	0.0520	$0.0552^{+0.0085}_{-0.0087}$	0.0580	$0.0576^{+0.0060}_{-0.0064}$
$w_{0,OSCILL}$	-1.39	$-1.17^{+0.07}_{-0.33}$	-0.83	$-1.30^{+0.34}_{-0.39}$
$w_{a,OSCILL}$	0.71	$1.25^{+0.08}_{-1.10}$	1.52	$0.18^{+1.30}_{-0.96}$
Derived Parameters				
H_0 / km s ⁻¹ Mpc ⁻¹ ..	83.41	$77.39^{+9.98}_{-8.03}$	69.09	$78.41^{+10.32}_{-14.85}$
σ_8	0.942	$0.901^{+0.082}_{-0.067}$	0.83	$0.89^{+0.29}_{-0.27}$
χ^2 Statistics				
χ^2_{min}		2768		30570
ΔAIC		-0.96		2.67
ΔBIC		15.12		19.21

TABLE S14. The values obtained from oscillatory reparametrisation model using either PR3 or PR4.

of the previous models, the Oscillatory model obtained slightly different values of the six Λ CDM parameters. This highlights the distinction between the two Planck datasets. This model retrieved lower values of w_{cdm} , w_b , n_s , $\ln 10^{10} A_s$, and $100\theta_s$, as well as a higher value of τ_{reio} . Fig. 12 shows the results of this model when combinations of early-time with late-time data were taken. The Oscillatory model produced degeneracies with the parameter $w_{a,OSCILL}$ when the data combination of PR4+CC+SN+SH0ES was used. However, when the other data combinations were taken this degeneracy is not seen. The addition of the late-time

Parameters	PR3		PR4	
	CC + SN+SH0ES		CC + SN+SH0ES	
	Best-fit	Mean	Best-fit	Mean
Sampled Parameters				
ω_b	0.02247	$0.02251^{+0.00016}_{-0.00015}$	0.02240	0.02234 ± 0.00012
ω_{cdm}	0.1184	$0.1188^{+0.0013}_{-0.0011}$	0.1173	0.1178 ± 0.0011
$100\theta_s$	1.04200	$1.04200^{+0.00028}_{-0.00030}$	1.04190	$1.04190^{+0.00025}_{-0.00026}$
$\ln(10^{10} A_s)$	3.056	$3.047^{+0.016}_{-0.018}$	3.050	3.039 ± 0.014
n_s	0.9701	$0.9686^{+0.0041}_{-0.0040}$	0.9721	$0.9700^{+0.0037}_{-0.0041}$
τ_{reio}	0.0626	$0.0566^{+0.0074}_{-0.0088}$	0.0642	$0.0588^{+0.0062}_{-0.0064}$
$w_{0, \text{OSCILL}}$	-0.878	$-0.904^{+0.042}_{-0.023}$	-0.836	$-0.863^{+0.039}_{-0.050}$
$w_{a, \text{OSCILL}}$	1.28	$1.23^{+0.27}_{-0.70}$	1.83	$1.51^{+0.43}_{-0.20}$
Derived Parameters				
H_0 / $\text{km s}^{-1} \text{Mpc}^{-1}$..	70.30	$70.74^{+0.66}_{-0.74}$	71.45	$70.80^{+0.70}_{-0.71}$
σ_8	0.837	$0.838^{+0.011}_{-0.012}$	0.841	0.833 ± 0.010
χ^2 Statistics				
χ^2_{min}		4092		31890
ΔAIC		-17.30		-18.00
ΔBIC		-1.23		-2.04

TABLE S15. The values that were achieved from the Oscillatory parameter when using CC and SN+SH0ES, either with PR3 or PR4 for the observational data: PR3+CC+SN+SH0ES; and PR4+CC+SN+SH0ES.

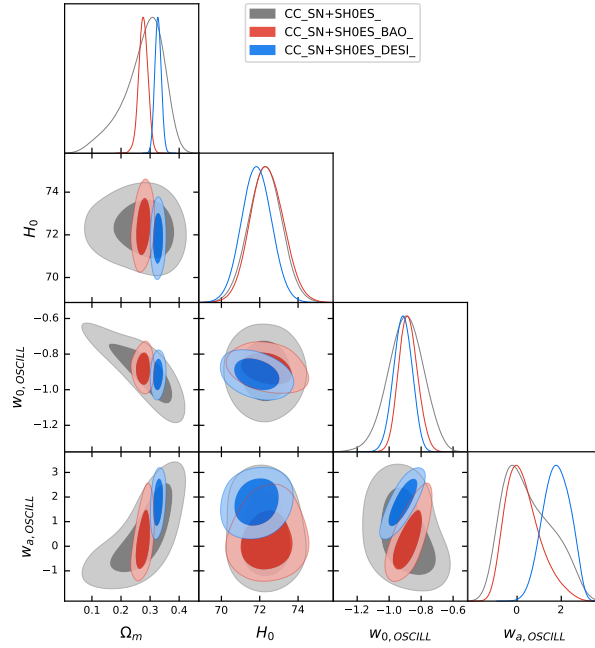


FIG. 10. The corner plot illustrates the Oscillatory parameterisation under different data combinations. The grey plot represents the use of CC + SN+SH0ES, while the red plot shows CC + SN+SH0ES + BAO data, and the blue plot depicts CC + SN+SH0ES + DESI data.

Parameters	PR3		PR4	
	CC + SN+SH0ES + DESI		CC + SN+SH0ES + DESI	
	Best-fit	Mean	Best-fit	Mean
Sampled Parameters				
ω_b	0.02251	0.02250 ± 0.00014	0.02219	0.02226 ± 0.00013
ω_{cdm}	0.1185	$0.1187^{+0.0010}_{-0.0011}$	0.11888	$0.11895^{+0.00094}_{-0.00099}$
$100\theta_s$	1.04180	1.04200 ± 0.00029	1.04190	1.04180 ± 0.00025
$\ln(10^{10} A_s)$	3.046	$3.046^{+0.015}_{-0.017}$	3.055	3.037 ± 0.014
n_s	0.9686	$0.9685^{+0.0040}_{-0.0038}$	0.9667	0.9669 ± 0.0035
τ_{reio}	0.0563	$0.0563^{+0.0075}_{-0.0085}$	0.0600	$0.0568^{+0.0059}_{-0.0061}$
$w_{0,OSCILL}$	-0.980	$-0.997^{+0.030}_{-0.027}$	-0.938	$-0.910^{+0.042}_{-0.043}$
$w_{a,OSCILL}$	-0.48	$-0.38^{+0.12}_{-0.02}$	0.92	$1.08^{+0.28}_{-0.33}$
Derived Parameters				
H_0 / km s ⁻¹ Mpc ⁻¹ ..	69.92	$69.87^{+0.61}_{-0.62}$	70.07	$69.85^{+0.60}_{-0.59}$
σ_8	0.826	$0.827^{+0.011}_{-0.012}$	0.836	0.831 ± 0.010
χ^2 Statistics				
χ^2_{min}		4112		31910
ΔAIC		-10.62		-8.80
ΔBIC		5.46		7.92

TABLE S16. The Oscillatory model's values when using each Planck data with CC, SN+SH0ES and DESI data: PR3+CC+SN+SH0ES+DESI; and PR4+CC+SN+SH0ES+DESI.

data was enough to constrain the complete degeneracy that was found when PR4 data was used. When the DESI data was added, the values of $w_{0,OSCILL}$, $w_{a,OSCILL}$, H_0 , and σ_8 were lowered. When the late-time data was added, the Oscillatory model turned from obtaining a phantom Universe to a quintessence one at low redshifts, as the late-time data lowered the values of $w_{0,OSCILL}$ to then change to a phantom Universe at high redshifts. From the four data combinations, it is seen that the oscillatory parameterisation produced the smallest 2D posteriors, PR4+CC+SN+SH0ES+DESI produced the smallest with the six Λ parameters, H_0 , and σ_8 , while for the $w_{0,OSCILL}$, and $w_{a,OSCILL}$ parameters, the oscillatory model obtained the smallest posteriors when the PR3+CC+SN+SH0ES+DESI data combination was considered.

In summary, the Oscillatory parameterisation is 1σ away from the Λ CDM model when PR4 and CC+SN+SH0ES data combination was taken. This model produced a phantom Universe when only Planck data was used, but then produced a quintessence Universe at low redshifts and a phantom Universe at high redshifts when late-time data was used and when late-time with early-time data was considered. This model showed that the DESI data showed to be a better dataset than the previous BAO data, while PR4 showed to be a better dataset with the six Λ CDM parameters, and the $w_{a,OSCILL}$ parameter. The PR3 showed to constrain the parameters $w_{0,OSCILL}$, H_0 , and σ_8 .

To conclude, this section showed the results that were obtained from four different dark energy equation of state parameters, showcased in tables displaying the mean, 1σ deviation, and best-fit, and in corner plots showing the marginalised 1-dimensional posteriors and the 2-dimensional 1σ and 2σ confidence-level posteriors. The constant model gives a phantom dark energy, the Logarithmic model generally prefers a quintessence dark energy, and the Oscillatory model showed a quintessence dark energy when late-time and late-time with early-time were considered, while when only early-time was taken, the models obtained a phantom dark energy. The tested models showed that generally, DESI and PR4 constrained the parameters better than the previously released datasets of BAO and PR3, respectively. However, for specific models, and for certain parameters, the PR3 showed to perform better than the newer Planck data.

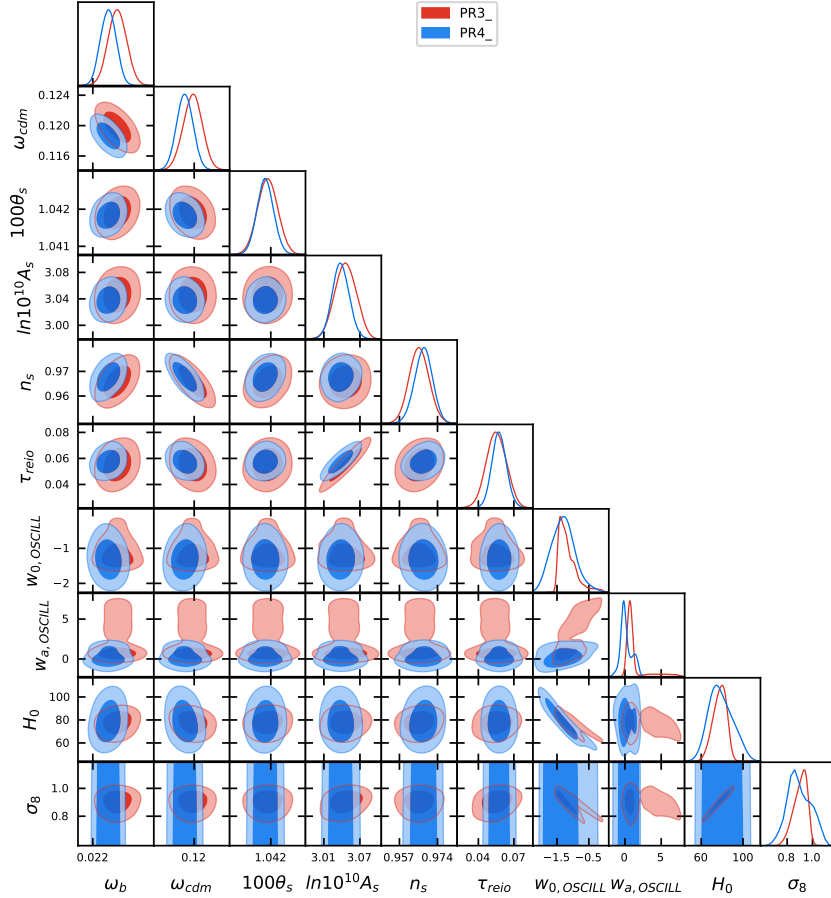


FIG. 11. The graph illustrates the two CMB data sets, unaffected by late-time data for the Oscillatory model. The red plot represents the use of PR3, while the blue plot corresponds to the use of PR4.

5. ANALYSIS OF RESULTS

In this section, the statistical performance of each parameterisation will be discussed, as well as how the models affect the six Λ CDM parameters. The Akaike Information Criterion (AIC) and Bayesian Information Criterion (BIC) statistics were taken as a measure to determine which parameterisation models are statistically better than the Λ CDM model and which ones are not.

Table S17 and Table S18 show the calculated values ΔAIC , which is $\text{AIC}_{\text{model}} - \text{AIC}_{\Lambda\text{CDM}}$ and the values of the ΔBIC which was calculated as $\text{BIC}_{\text{model}} - \text{BIC}_{\Lambda\text{CDM}}$, respectively. The first table shows that all models performed better than the standard model when Planck data was used with combinations of late-time data. When the latest Planck data was used, PR4, the Λ CDM model fit the data better than any of the tested models. On the other hand, when the previously released Planck data was considered, all the models, except for the Logarithmic model, fit the data better than the standard model. When only late-time data that included DESI was considered, all the models were statistically better than the Λ CDM model. From the AIC statistics, it can be seen that the model that fits the data the best depends on which data combination was picked. When looking at the ΔBIC , the only cases where any of the models fit the data better than the standard models were: the Oscillatory parameterisation when the PR3+CC+SN+SH0ES data combination and the PR4+CC+SN+SH0ES were considered; and the Logarithmic model when PR3+CC+SN+SH0ES+DDES data combination was used. From the BIC statistics, it can be concluded that the model that fit the data the best out of the five chosen parameterisations was the Oscillatory model.

Fig. 13 was generated showing the six Λ CDM parameters of the four w CDM models with respect to the standard model. It shows clearly the 1D marginalised posterior distributions and 2D contour plots for all

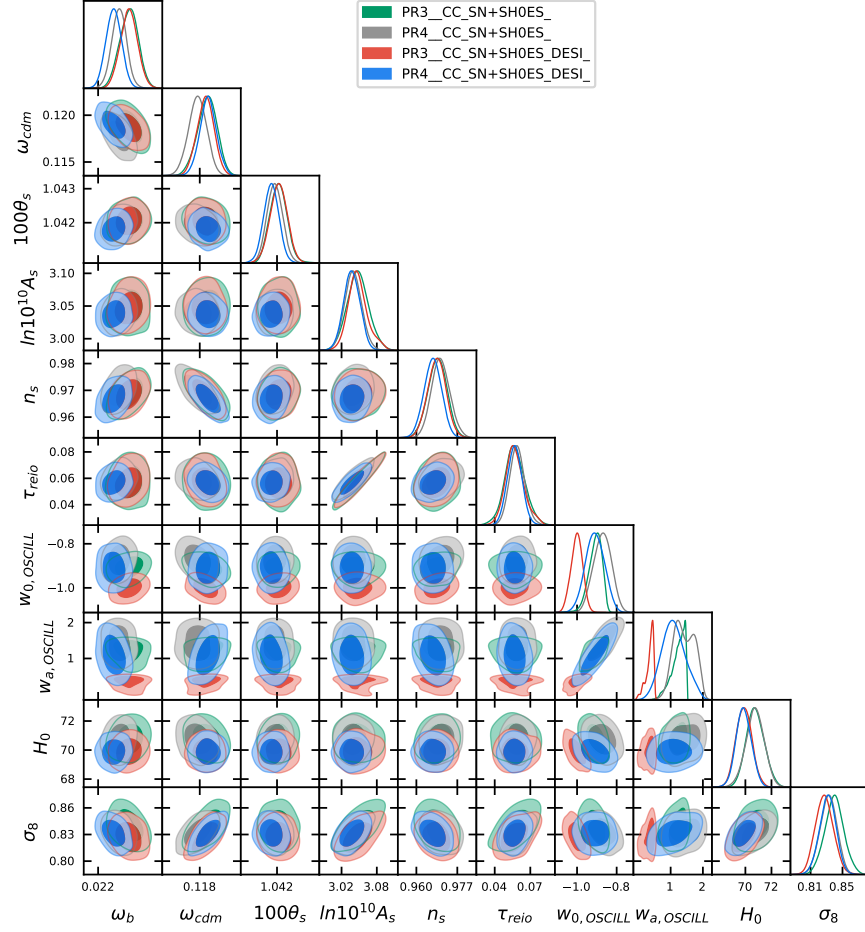


FIG. 12. The graph presents four overlapping corner plots of the Oscillatory model, incorporating two Planck data sets combined with various late-time data. The green plot represents PR3 + CC + SN+SH0ES, while the grey plot corresponds to PR4 + CC + SN+SH0ES. The red plot illustrates PR3 + CC + SN+SH0ES + DESI, and the blue plot depicts PR4 + CC + SN+SH0ES + DESI.

	CCSN	CCSNBAO	ALL	PR3	PR4	PR3/CCSN	PR4/CCSN	PR3/ALL	PR4/ALL
<i>w</i> CDM models									
Constant ..	0.91	-4.38	-0.65	-4.40	1.80	-4.44	-1.40	-3.24	-1.00
Quadratic ..	0.61	-0.38	-3.71	-2.08	3.60	-11.36	-8.40	-9.48	-6.40
Logarithmic .	0.93	4.02	-1.86	1.72	3.00	-11.54	-6.00	-25.52	-4.60
Oscillatory .	0.89	-2.31	-7.48	-0.96	2.67	-17.30	-18.00	-10.62	-8.80

TABLE S17. The table shows the values of the ΔAIC that were obtained from the four *w*CDM parametrisation model for each data combination, where CCSN is short for CC+SN+SH0ES, CCSNBAO refers to CC+SN+SH0ES+BAO, ALL is a notation for CC+SN+SH0ES+DESI, PR3/CCSN is short for PR3+CC+SN+SH0ES, PR4/CCSN refers to PR4+CC+SN+SH0ES, PR3/ALL represents PR3+CC+SN+SH0ES+DESI, and PR4/ALL represents PR4+CC+SN+SH0ES+DESI.

	CCSN	CCSNBAO	ALL	PR3	PR4	PR3/CCSN	PR4/CCSN	PR3/ALL	PR4/ALL
<i>w</i> CDM models									
Constant ..	6.37	1.09	4.81	10.04	9.90	3.60	6.96	4.80	7.36
Quadratic ..	13.52	1.09	7.22	14.00	20.32	4.72	8.32	6.60	10.32
Logarithmic .	13.84	14.95	9.06	17.80	19.61	4.54	10.72	-9.44	12.12
Oscillatory .	13.80	8.62	3.45	15.12	19.21	-1.23	-2.04	5.46	7.92

TABLE S18. A table showing the values of the ΔBIC that were obtained for each data combination of each *w*CDM model, where CCSN refers to the CC+SN+SH0ES, CCSNBAO refers to CC+SN+SH0ES+BAO, ALL is short for CC+SN+SH0ES+DESI, PR3/CCSN is short for PR3+CC+SN+SH0ES, PR4/CCSN is a notation for PR4+CC+SN+SH0ES, PR3/ALL represents PR3+CC+SN+SH0ES+DESI, and PR4/ALL refers to PR4+CC+SN+SH0ES+DESI.

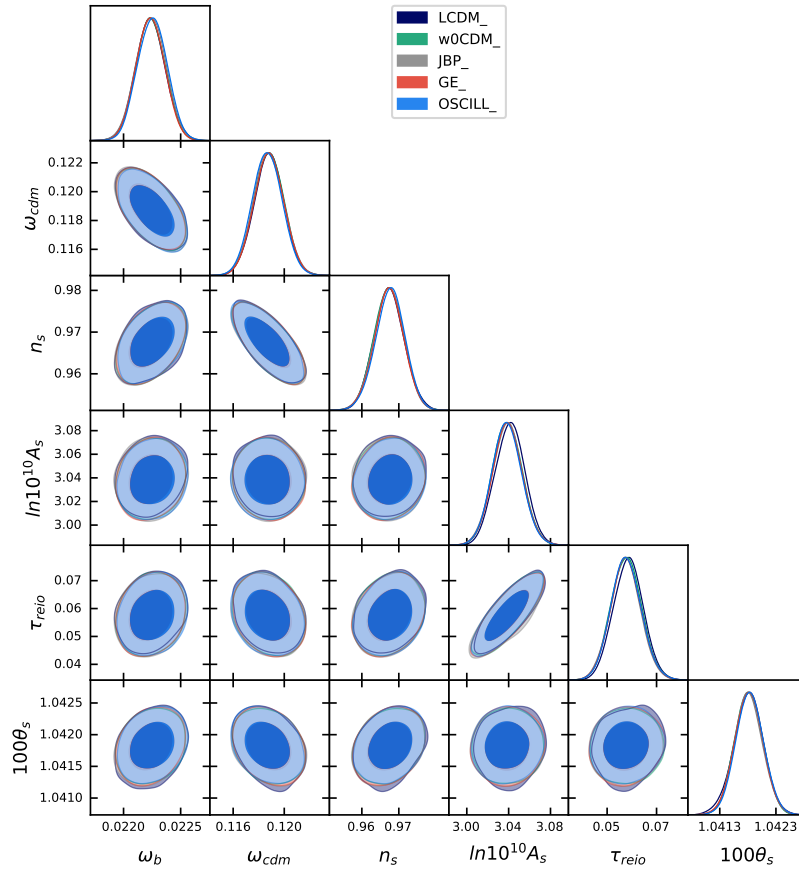


FIG. 13. The graph displays five overlapping corner plots, highlighting the six Λ CDM parameters extracted from the standard model alongside the four *w*CDM models when the PR4 data set was used.

considered dark energy models when using PR4 alone. There are no notable differences in the 1D and 2D posteriors between each tested model and the standard model. This shows that when early-time data was used, all the models have no effect on the early Universe as the models describe the same early Universe as the standard model. The constraints on the free cosmological parameters remain largely unaffected by the choice of dark energy parametrisation. Fig. 14 depicts the 1D marginalised posteriors and the 2D posteriors showing the 1σ and 2σ confidence levels of the six Λ CDM parameters for all the models, including the Λ CDM model when using PR4 with CC, SN+SH0ES, and DESI. When late time was added to the models, the

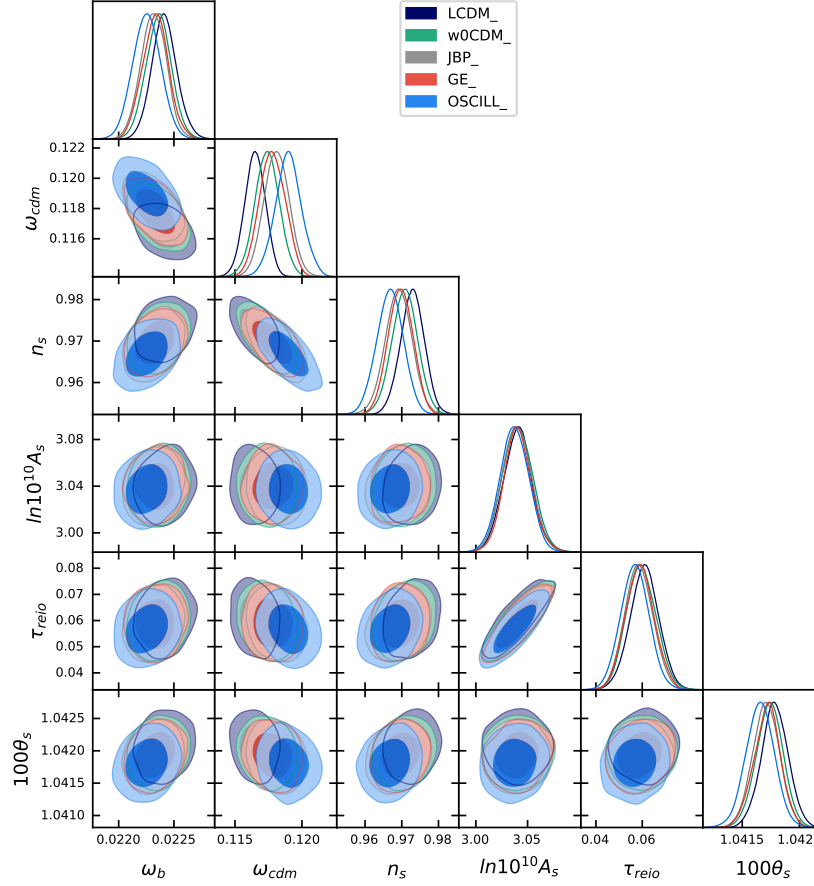


FIG. 14. A graph overlapping five corner plots, showing the six Λ CDM parameters that were achieved from the standard model and the four w CDM models that were tested in this project using the PR4+CC+SN+SH0ES+DESI data combination.

parameters obtained from the chosen models deviate from the standard model. Therefore, when late-time data was included in the w CDM models, effect the early Universe as is predicts the six Λ CDM parameters to be slightly different from the standard model. However, the 2D posteriors show that despite the deviation from the standard model, the models are all 1σ away from the Λ CDM model showing that despite this deviation, all the tested models limit to the standard model when it comes to the six Λ CDM parameters.

A whisker plot was generated as seen in Fig. 15, showcasing the parameters of w_0 , w_a except for the constant model, and H_0 when considering combinations of late time data. The same data combinations were used in section 4. The vertical coloured bars show the values of H_0 of past research: the cyan shows the value from Planck 2018 of $67.4 \pm 0.5 \text{ km s}^{-1} \text{ Mpc}^{-1}$ [2]; and the pink shows the value from SH0ES of $73.2 \pm 1.3 \text{ km s}^{-1} \text{ Mpc}^{-1}$ [27]. The figure indicates that, when relying solely on late-time data, the w CDM models consistently constrained w_0 , yielding very low uncertainties except for the constant model when DESI was incorporated. Regarding the w_a parameter, the logarithmic model achieved the lowest uncertainties and was closest to the standard model's value. On the contrary, the Oscillatory model and the Quadratic parameterisation had the largest uncertainty ranges. As for H_0 , the reparameterization models, generally attained an uncertainty range comparable to that of the Λ CDM model, except for when the logarithmic model was taken, as it consistently obtained high uncertainty bars for the H_0 parameter.

A whisker plot, presented in Fig. 16, illustrates the parameters w_0 and w_a , excluding the constant model, along with H_0 and σ_8 . This visualisation considers various late-time data combinations, consistent with those applied in Section 4. The vertical colored bars represent previous research values of H_0 and σ_8 : the green bar

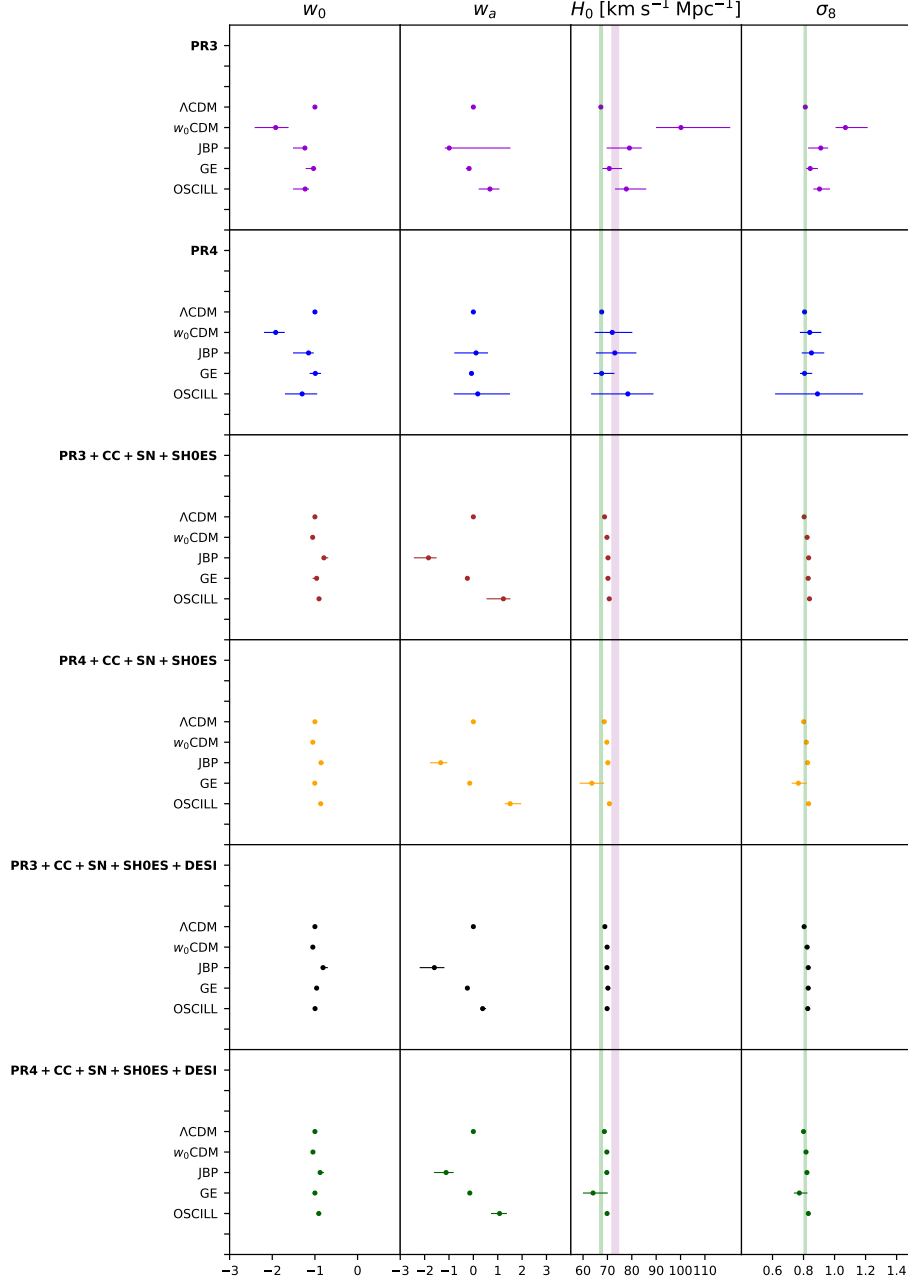


FIG. 15. The graph depicts a whisker plot [52] showcasing the results obtained from the four w CDM models and the Λ CDM model, when late-time data combinations were used in section 4. The code for the whisker plot was retrieved from: <https://github.com/lucavisinelli/H0TensionRealm.git>

indicates the Planck 2018 estimate of $H_0 = 67.4 \pm 0.5$ km s⁻¹Mpc⁻¹ and $\sigma_8 = 0.811 \pm 0.006$, while the pink bar corresponds to the SH0ES measurement of $H_0 = 73.2 \pm 1.3$ km s⁻¹Mpc⁻¹. Fig. 16 demonstrates that, overall, the constant parameterisation model exhibited larger uncertainties when relying solely on early-time data, compared to cases where combinations of late-time data were included. This highlights the necessity of late-time data for effectively constraining these four parameters. When late-time data was combined with CMB data, the variation in the parameters w_0 , H_0 , and σ_8 across models diminished. Specifically, when Planck data was supplemented with late-time data, w_0 values clustered around -1 , H_0 values centred

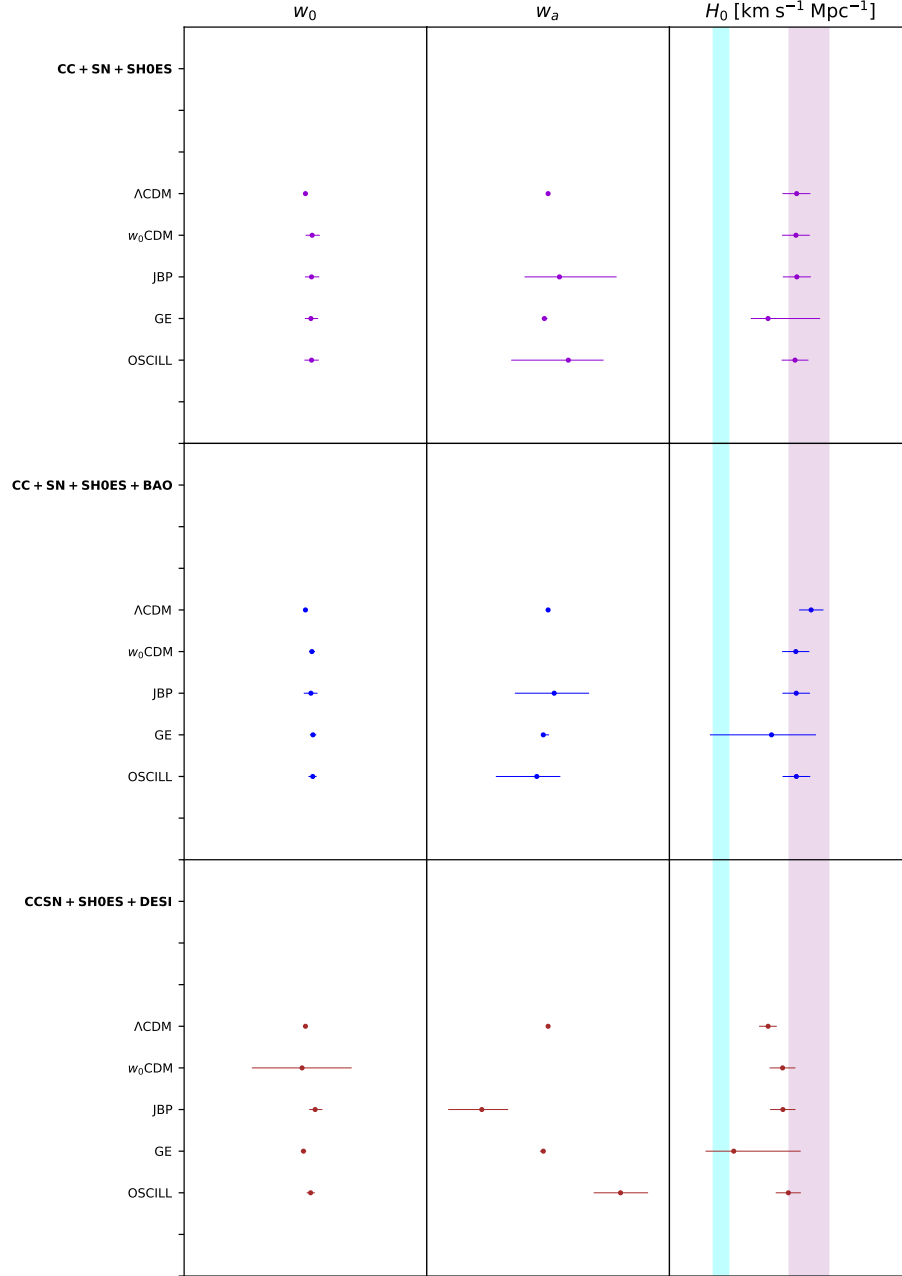


FIG. 16. A whisker plot [52] depicting the results obtained from the four w CDM models and the Λ CDM model, when early-time data with combinations of late-time data that were used in section 4.

around 70, and σ_8 values ranged between 0.8 and 0.9. The logarithmic model (GE) demonstrated higher uncertainties and yielded lower values for H_0 and σ_8 compared to other models when PR4 data was used. While the quadratic parameterisation obtained high uncertainties for w_a , when only early-time data was considered. Among all models, the w_0 CDM model recorded the highest uncertainties when solely utilising Planck 2018 data, particularly for the H_0 parameter. The Oscillatory model had obtained significantly large uncertainties with all four parameters when PR4 was used. As depicted in Fig. 16, the w_a parameter exhibited significant variation depending on the model and the data combination employed.

In conclusion, this section showed the Δ AIC and Δ BIC of the tested models, from them, it was deduced

Name of w CDM parametrisation model	Equation of state of dark energy w
Constant model	$w_{w0CDM}(a) = w_{0,w0CDM}$
Quadratic model	$w_{JBP}(a) = w_{0,JBP} + w_{a,JBP} a(1 - a)$
Logarithmic model	$w_{GE}(a) = w_{0,GE} - w_{a,GE} \ln(a)$
Oscillatory model	$w_{OSCILL}(a) = w_{0,OSCILL} + w_{a,OSCILL} [a \sin(\frac{1}{a}) - \sin(1)]$

TABLE S19. A table showing the list of models that were considered and their respective equation of state of dark energy w .

that with respect to the AIC which model fit the data the best varied depending on the data combination while the BIC showed that the Oscillatory parameterisation generally fit the data combinations better than the other chosen models. The AIC and BIC also showed that for certain data combinations, the tested models performed better than the Λ CDM model. Two overlapping graphs of the six Λ CDM parameters of the models and the standard model were generated, demonstrating that when early-time data was used, the chosen w CDM models do not affect the six Λ CDM parameters. However, when late-time data is added, deviations from the standard model are seen. It is important to note that despite this deviation, the tested models remain 1σ away from the standard model. Two whisker plots were also shown, and it was concluded that the uncertainties decrease when early-time and late-time data are used together as opposed to using late-time or early-time data by themselves.

6. SUMMARY AND CONCLUSIONS

Dark energy remains one of the greatest mysteries in modern cosmology, nearly two decades after its detection as the driving force behind the accelerated expansion of the Universe. The simplest and most widely accepted explanation is the Λ CDM cosmological model. While Λ CDM has proven successful in describing late-time cosmic acceleration and the Cosmic Microwave Background radiation, it has also raised significant tensions. The cosmological constant problem, related to discrepancies between theoretical predictions and observational estimates, remains one of the most profound challenges. Similarly, the cosmic coincidence problem, which questions why dark matter and dark energy densities are of comparable magnitude in the present cosmic epoch, has motivated the search for alternative models beyond Λ CDM. The pursuit of such alternatives gained momentum when discrepancies in H_0 estimations within Λ CDM were observed across different observational probes, exceeding 4 standard deviations. One potential approach to addressing these issues and because the precise nature of dark energy remains unknown, various forms of dark energy equation of state parameter that differs from $w = -1$ were explored. Specifically, five well-known dynamical dark energy models were investigated, aiming to assess their impact on the H_0 tension and the σ_8 tension in light of the latest Cosmic Microwave Background measurements from Planck 2020. In addition to the Planck data set, the Cosmic Chronometers, Pantheon+, Baryon Acoustic Oscillations, Dark Energy Spectroscopic Instrument, and local measurements of H_0 from SH0ES, as well as earlier CMB constraints from Planck 2018, to evaluate how cosmological constraints have evolved over time.

Our analysis focuses on four dark energy models: the constant model; the Quadratic model; the Logarithmic model; and the Oscillatory model. The equation of state for each model can be found in Table S19. Table S1-Table S16 present the best-fit and mean values of the six Λ CDM parameters, w_0 , w_a , H_0 , and σ_8 . Additionally, the triangular plots for the constant model, the Quadratic model, the Logarithmic model, and the Oscillatory model corresponding to CC+SN+SH0ES, CC+SN+SH0ES+BAO, CC+SN+SH0ES+DESI, Planck 2018, Planck 2020, Planck 2018 + CC+SN+SH0ES, Planck 2020+CC+SN+SH0ES, Planck 2018 + CC+SN+SH0ES+DESI, and Planck 2020+CC+SN+SH0ES+DESI are displayed in Fig 1-Fig. 12. Results indicate that for the constant model, the best-fit values of the dark energy equation of state parameter w , lie within the phantom regime. For the quadratic model, the logarithmic model, and the Oscillatory model, the mean values of w , lie within the quintessence regime at low redshifts but then shift to a phantom Universe at high redshifts. When only early-time data was used, the Quadratic, and the Oscillatory parameterisations showed a preference for a phantom Universe. When comparing the new datasets of DESI and PR4 to their

previously released data of BAO and PR3, the models showed that generally, the DESI and PR4 data performed better than BAO and PR3, respectively, as the 2D posteriors and the 1D marginalised posteriors were smaller when DESI or PR4 were used. There were some exceptions to this as the Oscillatory parameterisation, as when PR4 was considered by itself, the model obtained a completely degenerate σ_8 , and the posteriors of H_0 as well as $w_{0,OSCILL}$ were larger than when PR3 was used. The oscillatory parameterisation also produced larger posteriors when PR4 was used together with late-time for the parameters $w_{0,OSCILL}$, and $w_{a,OSCILL}$ than when PR3 was used with late-time.

The Akaike Information Criterion (AIC) and Bayesian Information Criterion (BIC) statistics were used, and the values that were calculated for each model for each data combination were displayed in Table S17 and Table S18. From the values of the ΔAIC , it was deduced that when using Planck data with combinations of late-time data, the models fit the data better than the Λ CDM model. This indicates that the tested models could be statistically better than the standard model and could result in a better value of H_0 and σ_8 and lessen the tensions with the two parameters. When the values of the ΔBIC were analysed, it was concluded that generally the Oscillatory model had the lowest values out of the five parameterisation models, indicating that the Oscillatory model was statistically the best model out of all of them. Negative values of ΔBIC were found with the Logarithmic model, and the Oscillatory model when specific data combinations were taken.

Fig. 13 and Fig. 14 were rendered to analyse the six Λ CDM parameters for all the chosen models with respect to the Λ CDM model when using PR4 only and then when using PR4+CC+SN+SH0ES+DESI, respectively. From the plots, it was decided that the chosen models did not have any effect on the six Λ CDM parameters when only early-time data was used. This implies that when using early-time data, the models do not affect the CMB power spectrum. When late-time data was added seen in Fig. 14, the six Λ CDM parameters obtained from the tested models are no longer the same as the standard model. However, the deviation from the standard model is 1σ for all the w CDM models showing that even though there is a deviation from the standard model, all the tested models limit to the Λ CDM model for the six Λ CDM parameters.

Two whisker plots were generated, as seen in Fig. 15 and Fig. 16, showing the w_0 , w_a , H_0 and σ_8 in the last figure for all data combinations that were used in section 4. From the two figures, it was concluded that the chosen models obtained large uncertainties when Planck data or late-time data by themselves are used. However, when late-time and early-time data are used together, the uncertainties are significantly lessened. This showed that late-time data is required for the w CDM models to give accurate values of the parameters and consequently an accurate description of the early and late Universe.

In summary, the analysis of this study showed how the w CDM models do not deviate so much from the Λ CDM model. It was seen that the tested models fit the older Planck data better than the newer one. This could be due to the newer model having less uncertainties than its predecessor. This study indicates that the tested dark energy models can align with the observational data. However, Bayesian analysis suggests that Λ CDM model remains the preferred model. A potential direction for further research could involve exploring a more general framework in which the sound speed of dark energy varies instead of remaining constant. This approach may shed light on the fundamental characteristics of dark energy models, and is reserved for future investigation. The code, figures, and values computed in this research can be found in the Github link: <https://github.com/kathleenUni/Update-of-wCDM-models/blob/main/README.md>.

ACKNOWLEDGMENTS

This article is also based upon work from COST Action CA21136 Addressing observational tensions in cosmology with systematics and fundamental physics (CosmoVerse) supported by COST (European Cooperation in Science and Technology). It was funded by the ENDEAVOUR II scholarship scheme offered by the Government of Malta Ministry for Education, Sport, Youth, Research and Innovation (MEYR). MEYR was not involved in any capacity in relation to the study design, collection, analysis and interpretation of data, writing of the report and decision to submit the article for publication. KS would also like to acknowledge Glenn Wallace for the help in the implementation of the Oscillatory parameterisation.

LIST OF FIGURES

1	The graph presents three overlapping corner plots of the constant model, utilising only late-time data. The grey plot represents CC + SN+SH0ES, the red plot corresponds to CC + SN+SH0ES + BAO, and the blue plot illustrates CC + SN+SH0ES + DESI.	9
2	The graph shows the w CDM model, with PR3 represented in red and PR4 in blue.	10
3	The graph depicts the constant model under different data combinations. The green plot represents CC + SN+SH0ES with PR3, while the grey plot corresponds to PR4. When CC + SN+SH0ES + DESI is used, the red plot depicts PR3, and the blue plot represents PR4... ..	11
4	A graph depicting the quadratic model when late-time data combinations were taken. The grey corner plot shows the model when CC, and SN+SH0ES data combination was considered, the red corner plot shows the model when the CC, SN+SH0ES, and BAO data combination was used, and the blue corner plot shows the parameterisation when CC, SN+SH0ES, and DESI data were taken.	13
5	A graph showing the results of the quadratic parameterisation when using PR3, shown in the red corner plot, and when considering the PR4 data set shown in the blue corner plot.	14
6	A graph showing the quadratic parameterisation when combinations of early-time and late-time data were considered. The green plot shows when PR3, CC, and SN+SH0ES were taken, the grey plot depicts when PR4, CC, and SN+SH0ES were used, the red plot displays the results obtained from when PR3, CC, SN+SH0ES, and DESI were taken, and the blue plot shows when PR4, CC, SN+SH0ES, and DESI were considered.	15
7	The graph represents the Logarithmic model using only late-time data. The grey plot corresponds to CC + SN+SH0ES, the red plot illustrates CC + SN+SH0ES + BAO, and the blue plot depicts CC + SN+SH0ES + DESI.	17
8	The Logarithmic parameterisation is depicted using observational data, with PR4 represented in the blue corner plot and PR3 shown in the red corner plot.	19
9	The graph shows the logarithmic model using late-time data. The green plot represents the model with CC and SN+SH0ES alongside PR3, while the grey plot corresponds to PR4. When DESI is incorporated into both data combinations, the red plot depicts PR3 + CC + SN+SH0ES + DESI, and the blue plot represents PR4 + CC + SN+SH0ES + DESI.	20
10	The corner plot illustrates the Oscillatory parameterisation under different data combinations. The grey plot represents the use of CC + SN+SH0ES, while the red plot shows CC + SN+SH0ES + BAO data, and the blue plot depicts CC + SN+SH0ES + DESI data.	22
11	The graph illustrates the two CMB data sets, unaffected by late-time data for the Oscillatory model. The red plot represents the use of PR3, while the blue plot corresponds to the use of PR4.	24
12	The graph presents four overlapping corner plots of the Oscillatory model, incorporating two Planck data sets combined with various late-time data. The green plot represents PR3 + CC + SN+SH0ES, while the grey plot corresponds to PR4 + CC + SN+SH0ES. The red plot illustrates PR3 + CC + SN+SH0ES + DESI, and the blue plot depicts PR4 + CC + SN+SH0ES + DESI.	25
13	The graph displays five overlapping corner plots, highlighting the six Λ CDM parameters extracted from the standard model alongside the four w CDM models when the PR4 data set was used.	26
14	A graph overlapping five corner plots, showing the six Λ CDM parameters that were achieved from the standard model and the four w CDM models that were tested in this project using the PR4+CC+SN+SH0ES+DESI data combination.	27
15	The graph depicts a whisker plot [52] showcasing the results obtained from the four w CDM models and the Λ CDM model, when late-time data combinations were used in section 4. The code for the whisker plot was retrieved from: https://github.com/lucavisinelli/H0TensionRealm.git	28
16	A whisker plot [52] depicting the results obtained from the four w CDM models and the Λ CDM model, when early-time data with combinations of late-time data that were used in section 4.	29

LIST OF TABLES

S1	The values of the constant model using different late-time data combinations: CC and SN+SH0ES; CC, SN+SH0ES, and BAO; and CC, SN+SH0ES, and DESI.	7
S2	The values of the constant model obtained from the chosen simulations when only Planck data, PR3 and PR4 were used.	7
S3	The values of the constant model obtained from the two Planck data when CC and SN+SH0ES data were added: PR3+CC+SN+SH0ES; and PR4+CC+SN+SH0ES.	8
S4	The values of the constant model obtained from the two Planck data when DESI was added to the CC and SN+SH0ES data: PR3+CC+SN+SH0ES+DESI; and PR4+CC+SN+SH0ES+DESI.	8
S5	The values of the JBP model when using only late-time data.	11
S6	The values of the JBP model using the two Planck data sets: PR3 or PR4.	12
S7	The values obtained from the JBP model when using PR3 and PR4 with CC and SN+SH0ES data.	12
S8	Values of the quadratic model obtained from PR3 + CC + SN+SH0ES + DESI and PR4 + CC + SN+SH0ES + DESI.	13
S9	The values of the Logarithmic model using different late-time data combinations: CC and SN+SH0ES; CC, SN+SH0ES, and BAO; and CC, SN+SH0ES, and DESI.	16
S10	The values of the GE model when only early-time data of PR3 and PR4 were used.	16
S11	The values of the logarithmic model when using PR3 and PR4 with CC and SN+SH0ES data: PR3+CC+SN+SH0ES; and PR4+CC+SN+SH0ES.	17
S12	Values of the GE model obtained from the two Planck data with CC, SN+SH0ES and DESI data: PR3+CC+SN+SH0ES+DESI; and PR4+CC+SN+SH0ES+DESI.	18
S13	The values retrieved from the Oscillatory model using different late-time data combinations: CC and SN+SH0ES; CC, SN+SH0ES, and BAO; and CC, SN+SH0ES, and DESI.	21
S14	The values obtained from oscillatory reparametrisation model using either PR3 or PR4.	21
S15	The values that were achieved from the Oscillatory parameter when using CC and SN+SH0ES, either with PR3 or PR4 for the observational data: PR3+CC+SN+SH0ES; and PR4+CC+SN+SH0ES.	22
S16	The Oscillatory model's values when using each Planck data with CC, SN+SH0ES and DESI data: PR3+CC+SN+SH0ES+DESI; and PR4+CC+SN+SH0ES+DESI.	23
S17	The table shows the values of the ΔAIC that were obtained from the four w CDM parametrisation model for each data combination, where CCSN is short for CC+SN+SH0ES, CCSNBAO refers to CC+SN+SH0ES+BAO, ALL is a notation for CC+SN+SH0ES+DESI, PR3/CCSN is short for PR3+CC+SN+SH0ES, PR4/CCSN refers to PR4+CC+SN+SH0ES, PR3/ALL represents PR3+CC+SN+SH0ES+DESI, and PR4/ALL represents PR4+CC+SN+SH0ES+DESI.	25
S18	A table showing the values of the ΔBIC that were obtained for each data combination of each w CDM model, where CCSN refers to the CC+SN+SH0ES, CCSNBAO refers to CC+SN+SH0ES+BAO, ALL is short for CC+SN+SH0ES+DESI, PR3/CCSN is short for PR3+CC+SN+SH0ES, PR4/CCSN is a notation for PR4+CC+SN+SH0ES, PR3/ALL represents PR3+CC+SN+SH0ES+DESI, and PR4/ALL refers to PR4+CC+SN+SH0ES+DESI.	26
S19	A table showing the list of models that were considered and their respective equation of state of dark energy w	30

GLOSSARY

AIC: Akaike Information Criterion. 7, 8, 11–13, 16–18, 21–25, 29–31, 33

ALL: CC+SN+SH0ES+DESI. 25, 26, 33

BAO: Baryonic Acoustic Oscillations. 1, 2, 5–7, 9–11, 13, 15–17, 19–23, 25, 26, 30–33

BIC: Bayesian Information Criterion. 7, 8, 11–13, 16–18, 21–24, 26, 29–31, 33

BOSS: Baryon Oscillation Spectroscopic Survey. 5

CC: Cosmic Chronometers. 1, 2, 5–27, 30–33

CLASS: Cosmic Linear Anisotropy Solving System. 6

CMB: Cosmic Microwave Background. 1, 2, 4, 24, 28, 30, 32

DES: Dark Energy Survey. 5

DESI: Dark Energy Spectroscopic Instrument. 2, 5–11, 13–27, 30–33

ELG: Emission-line Galaxies. 5

FLRW: Friedmann-Lemaître-Robertson-Walker. 2, 3

GE: G. Efstathiou. 16, 18, 33

JBP: Jassal-Bagla-Padmanabhan. 4, 11, 12, 33

LRG: Luminous Red Galaxies. 5

MCMC: Markov Chain Monte Carlo. 6

PR3: Planck 2018. 4, 6–8, 10–26, 31–33

PR3/ALL: PR3+CC+SN+SH0ES+DESI. 25, 26, 33

PR4: Planck 2020. 4, 6–27, 29–33

PR4/ALL: PR3+CC+SN+SH0ES+DESI. 25, 26, 33

SDSS: Sloan Digital Sky Survey. 5

SH0ES: Supernovae H0 for the Equation of State. 2, 5, 30

SN: Type 1a Supernovae. 5

SN+: Pantheon+. 2, 5

SN+SH0ES: Pantheon+ and Supernovae H0 for the Equation of State. 5–27, 30–33

-
- [1] Bernal, J. L.; Verde, L.; Riess, A. G. *JCAP* **2016**, *10*, 019, <https://doi.org/10.48550/arXiv.1607.05617>.
 - [2] Aghanim, N.; others *Astron. Astrophys.* **2020**, *641*, A6, <https://doi.org/10.48550/arXiv.1807.06209>.
 - [3] Riess, A. G.; others *Astron. J.* **1998**, *116*, 1009–1038, <https://doi.org/10.48550/arXiv.astro-ph/9805201>.
 - [4] Perlmutter, S.; others *Bull. Am. Astron. Soc.* **1997**, *29*, 1351, <https://doi.org/10.48550/arXiv.astro-ph/9812473>.
 - [5] Hackmann, E.; Huckfeldt, M.; Lämmerzahl, C.; Philipp, D.; Rievers, B. **2025**, <https://doi.org/10.48550/arXiv.2503.09272>.
 - [6] Garcia-Quintero, C.; Ishak, M.; Fox, L.; Lin, W. *Phys. Rev. D* **2019**, *100*, 123538, <https://doi.org/10.48550/arXiv.1910.01608>.
 - [7] Wu, W. L. K.; Motloch, P.; Hu, W.; Raveri, M. *Phys. Rev. D* **2020**, *102*, 023510, <https://doi.org/10.48550/arXiv.2004.10207>.
 - [8] Benaoum, H. B.; Yang, W.; Pan, S.; Di Valentino, E. *Int. J. Mod. Phys. D* **2022**, *31*, 2250015, <https://doi.org/10.48550/arXiv.2008.09098>.
 - [9] Nojiri, S.; Odintsov, S. D. *eConf* **2006**, *C0602061*, 06, <https://doi.org/10.48550/arXiv.hep-th/0601213>.
 - [10] Capozziello, S.; De Laurentis, M. *Phys. Rept.* **2011**, *509*, 167–321, <https://doi.org/10.48550/arXiv.1108.6266>.
 - [11] Di Valentino, E. *Nature Astron.* **2017**, *1*, 569–570, <https://doi.org/10.48550/arXiv.1709.04046>.
 - [12] Marcondes, R. J. F.; Pan, S. **2017**, <https://doi.org/10.48550/arXiv.1711.06157>.
 - [13] Vagnozzi, S.; Dhawan, S.; Gerbino, M.; Freese, K.; Goobar, A.; Mena, O. *Phys. Rev. D* **2018**, *98*, 083501, <https://doi.org/10.48550/arXiv.1801.08553>.
 - [14] Chevallier, M.; Polarski, D. *Int. J. Mod. Phys. D* **2001**, *10*, 213–224, <https://doi.org/10.48550/arXiv.astro-ph/0208512>.
 - [15] Linder, E. V. *Phys. Rev. Lett.* **2003**, *90*, 091301, <https://doi.org/10.48550/arXiv.astro-ph/0208512>.
 - [16] Jassal, H. K.; Bagla, J. S.; Padmanabhan, T. *Phys. Rev. D* **2005**, *72*, 103503, <https://doi.org/10.48550/arXiv.astro-ph/0506748>.
 - [17] Yang, W.; Di Valentino, E.; Pan, S.; Wu, Y.; Lu, J. *Mon. Not. Roy. Astron. Soc.* **2021**, *501*, 5845–5858, <https://doi.org/10.48550/arXiv.2101.02168>.
 - [18] Efstathiou, G. *Mon. Not. Roy. Astron. Soc.* **1999**, *310*, 842–850, <https://doi.org/10.48550/arXiv.astro-ph/9904356>.
 - [19] Ma, J.-Z.; Zhang, X. *Phys. Lett. B* **2011**, *699*, 233–238, <https://doi.org/10.48550/arXiv.1102.2671>.
 - [20] Pan, S.; Saridakis, E. N.; Yang, W. *Phys. Rev. D* **2018**, *98*, 063510, <https://doi.org/10.48550/arXiv.1712.05746>.
 - [21] Linder, E. V.; Huterer, D. *Phys. Rev. D* **2005**, *72*, 043509, <https://doi.org/10.48550/arXiv.astro-ph/0505330>.
 - [22] De Felice, A.; Nesseris, S.; Tsujikawa, S. *JCAP* **2012**, *05*, 029, <https://doi.org/10.48550/arXiv.1203.6760>.
 - [23] Aghanim, N.; others *Astron. Astrophys.* **2020**, *641*, A8, <https://doi.org/10.48550/arXiv.1807.06210>.
 - [24] Carron, J.; Mirmelstein, M.; Lewis, A. *JCAP* **2022**, *09*, 039, <https://doi.org/10.48550/arXiv.2206.07773>.
 - [25] Favale, A.; Gómez-Valent, A.; Migliaccio, M. *Mon. Not. Roy. Astron. Soc.* **2023**, *523*, 3406–3422, <https://doi.org/10.48550/arXiv.2301.09591>.
 - [26] Scolnic, D.; others *Astrophys. J.* **2022**, *938*, 113, <https://doi.org/10.48550/arXiv.2112.03863>.
 - [27] Sharon, A.; Kushnir, D.; Yuan, W.; Macri, L.; Riess, A. *Monthly Notices of the Royal Astronomical Society* **2024**, *528*, 6861–6880, <http://dx.doi.org/10.1093/mnras/stae451>.
 - [28] Haridasu, B. S.; Luković, V. V.; Vittorio, N. *JCAP* **2018**, *05*, 033, <https://doi.org/10.48550/arXiv.1711.03929>.
 - [29] Copeland, E. J.; Sami, M.; Tsujikawa, S. *Int. J. Mod. Phys. D* **2006**, *15*, 1753–1936, <https://doi.org/10.48550/arXiv.hep-th/0603057>.
 - [30] Malik, K. A.; Wands, D. *Phys. Rept.* **2009**, *475*, 1–51, <https://doi.org/10.48550/arXiv.0809.4944>.
 - [31] Ma, C.-P.; Bertschinger, E. *Astrophys. J.* **1995**, *455*, 7–25, <https://doi.org/10.48550/arXiv.astro-ph/9506072>.
 - [32] Weller, J.; Lewis, A. M. *Mon. Not. Roy. Astron. Soc.* **2003**, *346*, 987–993, <https://doi.org/10.48550/arXiv.astro-ph/0307104>.
 - [33] Erickson, J. K.; Caldwell, R. R.; Steinhardt, P. J.; Armendariz-Picon, C.; Mukhanov, V. F. *Phys. Rev. Lett.* **2002**, *88*, 121301, <https://doi.org/10.48550/arXiv.astro-ph/0112438>.
 - [34] Hannestad, S. *Phys. Rev. D* **2005**, *71*, 103519, <https://doi.org/10.48550/arXiv.astro-ph/0504017>.
 - [35] Nunes, R. C.; Pan, S.; Saridakis, E. N. *Phys. Rev. D* **2016**, *94*, 023508, <https://doi.org/10.48550/arXiv.1605.01712>.
 - [36] Anagnostopoulos, F. K.; Basilakos, S. *Phys. Rev. D* **2018**, *97*, 063503, <https://doi.org/10.48550/arXiv.1709.02356>.
 - [37] Moresco, M.; Pozzetti, L.; Cimatti, A.; Jimenez, R.; Maraston, C.; Verde, L.; Thomas, D.; Citro, A.; Tojeiro, R.;

- Wilkinson, D. *JCAP* **2016**, *05*, 014, <https://doi.org/10.48550/arXiv.1601.01701>.
- [38] Brout, D.; others *Astrophys. J.* **2022**, *938*, 110, <https://doi.org/10.48550/arXiv.2202.04077>.
- [39] Fernández-García, E.; Betancort-Rijo, J. E.; Prada, F.; Ishiyama, T.; Klypin, A. **2024**, <https://doi.org/10.48550/arXiv.2406.13736>.
- [40] Carvalho, G. C.; Bernui, A.; Benetti, M.; Carvalho, J. C.; Alcaniz, J. S. *Phys. Rev. D* **2016**, *93*, 023530, <https://doi.org/10.48550/arXiv.1507.08972>.
- [41] Carvalho, G. C.; Bernui, A.; Benetti, M.; Carvalho, J. C.; de Carvalho, E.; Alcaniz, J. S. <https://doi.org/10.48550/arXiv.1709.00271>, journal = "Astropart. Phys.", volume = "119", pages = "102432", year = "2020".
- [42] Abbott, T.; others *Mon. Not. Roy. Astron. Soc.* **2016**, *460*, 1270–1299, <https://doi.org/10.48550/arXiv.1601.00329>.
- [43] Alam, S.; others *Phys. Rev. D* **2021**, *103*, 083533, <https://doi.org/10.48550/arXiv.2007.08991>.
- [44] Alcaniz, J. S.; Carvalho, G. C.; Bernui, A.; Carvalho, J. C.; Benetti, M. *Fundam. Theor. Phys.* **2017**, *187*, 11–19, <https://doi.org/10.48550/arXiv.1611.08458>.
- [45] Adame, A. G.; others *JCAP* **2025**, *02*, 021, <https://doi.org/10.48550/arXiv.2404.03002>.
- [46] Collaboration, D. et al. DESI 2024 V: Full-Shape Galaxy Clustering from Galaxies and Quasars. 2025; <https://arxiv.org/abs/2411.12021>, <https://doi.org/10.48550/arXiv.2411.12021>.
- [47] Brinckmann, T.; Lesgourgues, J. **2018**, <https://doi.org/10.48550/arXiv.1804.07261>.
- [48] Audren, B.; Lesgourgues, J.; Benabed, K.; Prunet, S. *JCAP* **2013**, *1302*, 001, <https://doi.org/10.48550/arXiv.1210.7183>.
- [49] Lesgourgues, J. **2011**, <https://doi.org/10.48550/arXiv.1104.2932>.
- [50] Blas, D.; Lesgourgues, J.; Tram, T. *Journal of Cosmology and Astroparticle Physics* **2011**, *2011*, 034–034, <http://dx.doi.org/10.1088/1475-7516/2011/07/034>.
- [51] Lewis, A. GetDist: a Python package for analysing Monte Carlo samples. 2019; <https://arxiv.org/abs/1910.13970>.
- [52] Di Valentino, E.; Mena, O.; Pan, S.; Visinelli, L.; Yang, W.; Melchiorri, A.; Mota, D. F.; Riess, A. G.; Silk, J. *Class. Quant. Grav.* **2021**, *38*, 153001, <https://doi.org/10.48550/arXiv.2103.01183>.